The Astrophysical Journal, 744:128 (18pp), 2012 January 10 doi:10.1088/0004-637X/744/2/128

THE THREE-DIMENSIONAL STRUCTURE OF THE SMALL MAGELLANIC CLOUD

Smitha Subramanian[1,2] and Annapurni Subramaniam[1]
[1] Indian Institute of Astrophysics, Koramangala II Block, Bangalore-34, India
[2] Department of Physics, Calicut University, Calicut, Kerala, India
Received 2011 February 4; accepted 2011 September 16; published 2011 December 22

ABSTRACT

The three-dimensional structure of the inner Small Magellanic Cloud (SMC) is investigated using the red clump (RC) stars and the RR Lyrae stars (RRLS), which represent the intermediate-age and the old stellar populations of a galaxy. The *V*- and *I*-band photometric data from the OGLE III catalog are used for our study. The mean dereddened I_0 magnitude of the RC stars and the RRLS are used to study the relative positions of the different regions in the SMC with respect to the mean SMC distance. This shows that the northeastern part of the SMC is closer to us. The line-of-sight depth (front to back distance) across the SMC is estimated using the dispersion in the I_0 magnitudes of both the RC stars and the RRLS and found to be large (∼14 kpc) for both populations. The similarity in their depth distribution suggests that both of these populations occupy a similar volume of the SMC. The surface density distribution and the radial density profile of the RC stars suggest that they are more likely to be distributed in a nearly spheroidal system. The tidal radius estimated for the SMC system is ∼7–12 kpc. An elongation along the NE–SW direction is seen in the surface density map of the RC stars. The surface density distribution of the RRLS in the SMC is nearly circular. Based on all of the above results the observed structure of the SMC, in which both the RC stars and RRLS are distributed, is approximated as a triaxial ellipsoid. The parameters of the ellipsoid are obtained using the inertia tensor analysis. We estimated the axes ratio, inclination of the longest axis with the line of sight (i), and the position angle (ϕ) of the longest axis of the ellipsoid on the sky from the analysis of the RRLS. The analysis of the RC stars with the assumption that they are extended up to a depth of 3.5 times the sigma (width of dereddened I_0 magnitude distribution, corrected for intrinsic spread and observational errors) was also found to give similar axes ratio and orientation angles. The above estimated parameters depend on the data coverage of the SMC. Using the RRLS with equal coverage in all three axes (data within 3° in *X*-, *Y*-, and *Z*-axes), we estimated an axes ratio of 1:1.33:1.61 with $i = 2.^\circ6$ and $\phi = 70.^\circ2$. Our tidal radius estimates and the recent observational studies suggest that the full extent of the SMC in the *XY* plane is of the order of the front to back distance estimated along the line of sight. These results suggest that the structure of the SMC is spheroidal or slightly ellipsoidal. We propose that the SMC experienced a merger with another dwarf galaxy at ∼4–5 Gyr ago, and the merger process was completed in another 2–3 Gyr. This resulted in a spheroidal distribution comprising stars older than 2 Gyr.

Key words: galaxies: structure – Magellanic Clouds – stars: horizontal-branch – stars: variables: RR Lyrae

Online-only material: color figures

1. INTRODUCTION

The Small Magellanic Cloud (SMC), located at a distance of around 60 kpc, is one of the nearest galaxies. The SMC is characterized by a less pronounced bar than that seen in the Large Magellanic Cloud (LMC). It also has an eastern extension called the Wing. The Wing and the northeastern part of the bar are closer than the southern parts (Hatzidimitriou et al. 1993). A large line-of-sight depth was found in the outer and inner regions of the SMC by Gardiner & Hawkins (1991) and Subramanian & Subramaniam (2009), respectively.

In an extensive survey of variable stars in the SMC, Graham (1975) discovered 76 RR Lyrae stars (RRLS) in the field centered on the globular cluster, NGC 121. He found that the period distribution of the RRLS in the SMC is unlike that found anywhere in the Galaxy and closely resembles the distribution of variable stars in the Leo II dwarf galaxy. His studies also showed that these stars are distributed rather evenly and concentrated neither toward the bar nor toward the center of the SMC. He mentioned that the lack of strong stellar concentration is another property in common with the stellar populations in the dwarf spheroidal galaxies. Smith et al. (1992) and Soszyñski et al. (2002) also found an even and smooth distribution of RRLSs in the northeastern regions and the central 2.4 deg^2 regions of the SMC, respectively. Subramanian & Subramaniam (2009) used the RRLS data published by Soszyñski et al. (2002) to estimate the depth in the central regions of the SMC. They found that the depth estimated using the red clump (RC) stars and the RRLS is similar in the central regions of the SMC. They suggested that the RRLS and the RC stars in the central bar region of the SMC are born in the same location and occupy a similar volume in the galaxy. Soszyñski et al. (2010) presented a catalog of the RRLS in the SMC from the OGLE III survey. From the spatial distribution of the RRLS they suggested that the halo of the SMC is roughly circular in the sky. However, their density map of the RRLS revealed two maxima near the center of the SMC.

Zaritsky et al. (2000) showed that the older stellar populations (age >1 Gyr) in the SMC are distributed in a regular, smooth ellipsoid. Similar conclusions were drawn by Cioni et al. (2000) from the DENIS near-infrared survey. Maragoudaki et al. (2001) further investigated the dynamical origin of the bar using isodensity contour maps of stars with different ages. They found similar results for old stellar populations. A sample of 12 populous SMC clusters that possess RC stars is studied by Crowl et al. (2001) to determine the distances to them. The line-of-sight depth of the SMC is estimated as the standard

deviation (σ) of these distances. They found a 1σ depth of ≈6–12 kpc for the SMC. Viewing the SMC as a triaxial ellipsoid with R.A., decl., and line-of-sight depth as the three axes, they found an axes ratio of 1:2:4. From a spectroscopic study of 2046 red giant stars, Harris & Zaritsky (2006) found that the older stellar components of the SMC have a velocity dispersion of 27.5 km s^{-1} and a maximum possible rotation of 17 km s^{-1}. Their result is consistent with other kinematical studies based on the radial velocities of the planetary nebulae and carbon stars, which represent the old and intermediate-age stellar populations (Dopita et al. 1985; Suntzeff et al. 1986; Hatzidimitriou et al. 1997). This implies that the structure of the older stellar component of the SMC is a spheroidal/ellipsoidal that is supported by its velocity dispersion.

From the analysis of young stars (age < 200 Myr), Zaritsky et al. (2000) suggested that the irregular appearance of the SMC is due to recent star formation. As in the case of young stars, the large-scale H I morphology of the SMC obtained from the high-resolution H I observations (Stanimirović et al. 2004) is also quite irregular and does not show symmetry. The most prominent features are the elongation from the northeast to the southwest and the V-shaped concentration in the east. The H I observations also show that the SMC has a significant amount of rotation with a circular velocity of approximately 60 km s^{-1} (Stanimirović et al. 2004) and a large velocity gradient of 91 km s^{-1} in the southwest to 200 km s^{-1} in the northeast. Evans & Howarth (2008) obtained velocities for 2045 young (O, B, A) stars in the SMC and found a velocity gradient of similar slope as seen in the H I gas. Surprisingly though, they found a position angle (∼126°) for the line of maximum velocity gradient that is quite different from and almost orthogonal to that seen in the H I. Van der Marel et al. (2009) suggested that this difference in the position angles may be an artifact of the different spatial coverage of the two studies (Evans & Howarth 2008 did not observe in the northeast region where the H I velocities are the largest), since it would be difficult to find a physical explanation for a significant difference in kinematics between H I gas and young stars. The inclination of the SMC disk in which the young stars are believed to be distributed is estimated as $70° \pm 3°$ and $68° \pm 2°$ from the photometric studies of Cepheids by Caldwell & Coulson (1986) and Groenewegen (2000), respectively. The position angle of the line of nodes is estimated to be ∼148.°0.

Gardiner & Noguchi (1996) modeled the SMC as a two-component system consisting of a nearly spherical halo and a rotationally supported disk. The tidal radius of the SMC is estimated as 5 kpc according to their model. Their best fit to the distribution halo particles within a 5 kpc radius was in good agreement with the observed distributions of the old (>9 Gyr) and intermediate-age (2–9 Gyr) stellar populations in the SMC. The distribution of disk particles could reproduce the observed irregular distribution of young stars in the SMC. Bekki & Chiba (2008) suggested that a major merger event in the early stage of SMC formation caused the coexistence of a spheroidal stellar component and an extended rotating H I disk.

Both the observational and theoretical studies suggest that the old and the intermediate-age stellar populations in the SMC are distributed in a spheroidal/ellipsoidal component. Motivated by this result, here we study the RC stars and the RRLS in the inner SMC, which represent the intermediate-age and the old stellar populations, respectively. This study aims to understand the structure of the inner SMC and hence to quantitatively estimate the structural parameters.

The RC stars are core helium burning stars, which are metal rich and slightly more massive counterparts of the horizontal branch stars. They have tightly defined color and magnitude, and appear as an easily identifiable component in color–magnitude diagrams (CMDs). These properties of the RC stars make them a good proxy for determining the distance to a galaxy and also understanding the structure of a galaxy. Previously, many people have used the RC stars as a proxy for distance estimation (Stanek et al. 1998) to identify the structures in the LMC (Subramaniam 2003) and to estimate the orientation measurements of the LMC (Olsen & Salyk 2002; Subramanian & Subramaniam 2010). Subramanian & Subramaniam (2009) estimated the depth of both the LMC and the SMC using the dispersions in magnitude and color distributions of the RC stars.

The RRLS are metal-poor, low-mass, core-helium-burning stars that undergo radial pulsations. Their period of pulsation has a range of 0.2–1 day. The RRLS are excellent tracers of the oldest observable population of stars in a galaxy. The RRab-type stars have a constant mean magnitude and they are used for distance estimation (Borissova et al. 2009). The dispersion about the mean magnitude is a measure of the depth of the host galaxy. Subramaniam (2006) and Subramanian & Subramaniam (2009) used the dispersion of the RRab stars to estimate the line-of-sight depth of the LMC and SMC, respectively. Pejcha & Stanek (2009) studied the structure of the LMC stellar halo using the RRLS in the LMC.

In this paper, we estimate the structural parameters of the older component of the SMC from the analysis of the RC stars and the RRLS in the inner SMC. Udalski et al. (2008) presented the *V*- and *I*-band photometric data of the 16 deg^2 of the SMC from the OGLE III survey. The catalog of the SMC RRLS from the OGLE III survey is presented by Soszyñski et al. (2010). Both data sets are used in this study. The mean dereddened I_0 magnitudes of the RC stars and the RRLS are used to estimate the relative locations of different regions in the SMC with respect to the mean SMC distance. The dispersion in the mean magnitude is used to obtain the line-of-sight depth across the SMC.

The structure of the paper is as follows. The next section deals with the contribution of a heterogeneous population on the dereddened I_0 magnitudes of the RC stars and RRLS and also the dispersion in their mean magnitude. In Section 3, we explain the data and analysis of both the RC stars and the RRLS. The reddening map of the SMC is presented in Section 4. The results of our analysis are given in Section 5. The estimation of the structural parameters of the SMC is explained in detail in Section 6. The discussion and the conclusions are presented in Sections 7 and 8, respectively.

2. CONTRIBUTION OF HETEROGENEOUS POPULATION

Stanek et al. (1998) determined the distance to the Magellanic Clouds (MCs) as well as to the bulge of our Galaxy from the dereddened apparent magnitude of the RC stars, assuming a constant absolute *I*-band magnitude. Later Sarajedini (1999) and Cole (1998) claimed that the luminosity of the RC stars is highly influenced by the age and metallicity and must be accounted for in the determination of the distance. When the controversy regarding the use of RC stars as the absolute indicator continued, they were used to estimate relative distances between regions within the MCs. Olsen & Salyk (2002), Subramaniam (2003), and Subramanian & Subramaniam (2010) used them as relative distance indicators in their studies.

The RC stars in the SMC are a heterogeneous population and hence they would have a range of masses, ages, and metallicities. The density of stars in various locations will also vary with the local star formation rate as a function of time. These factors would contribute to the range of magnitude and color of the net population of the RC stars in any given location of the SMC and hence to the observed peak magnitude and dispersion. Girardi & Salaris (2001) simulated the RC stars in the SMC using the star formation history and age–metallicity relation from Pagel & Tautvaisiene (1998). They created synthetic CMDs of the SMC and the distributions of the RC stars were fitted using numerical analysis to obtain the mean and dispersion of the magnitude and color distributions. The model-predicted values are used in our study to account for the population effects of the RC stars. The estimated intrinsic widths of the color and magnitude distributions of the RC stars in the SMC are 0.03 mag and 0.076 mag, respectively.

The RRLS in the SMC are also a heterogeneous population with a range of ages, metallicities, and masses. There are small variations in their luminosities due to evolutionary effects. These factors could contribute to the observed dereddened magnitudes of these stars and also to the dispersion of magnitude within a sample. This is discussed in Section 3.2.

Apart from multiple populations in a given region, there could be variation in population and metallicity across the SMC. Cioni et al. (2006) did not find any different population or metallicity gradient near the central regions of the SMC. Tosi et al. (2008) obtained deep CMDs of six SMC inner regions with which to study the star formation history. The interesting fact they found about the six CMDs is the apparent homogeneity of the old stellar population populating the subgiant branch and the clump. This suggested that there is no large difference in age and metallicity among old stars in the inner SMC.

3. DATA AND ANALYSIS

3.1. Red Clump Stars

The OGLE III survey (Udalski et al. 2008) presented the *V*- and *I*-band photometric data of 16 deg^2 of the SMC consisting of about 35 million stars. We divided the observed region into 1280 regions with a bin size of 8.88×4.44 arcmin^2. The average photometric error of RC stars in the *I* and *V* bands is around 0.05 mag. Photometric data with errors less than 0.15 mag are considered for the analysis. For each sub-region the $(V-I)$ versus *I* CMD is plotted and the RC stars are identified. A sample CMD is shown in Figure 1. For all the regions, RC stars are found to be located well within the box shown in the CMD, with boundaries 0.65–1.35 mag in $(V-I)$ color and 17.5–19.5 mag in *I* magnitude. The number of RC stars identified in each sub-region ranges from 100 to 3000.

The RC stars occupy a compact region in the CMD. Their number distribution profiles resemble a Gaussian. The peak values of their color and magnitude distributions are used to obtain the mean dereddened RC magnitude and hence the mean line-of-sight distance to each sub-region in the SMC. The dispersions in the magnitude and color distribution of the RC stars are used to obtain the line-of-sight depth of each sub-region in the SMC.

To obtain the number distribution of the RC stars, they are binned in color and magnitude with a bin size of 0.01 and 0.025 mag, respectively. These distributions are fitted with a Gaussian + quadratic polynomial. The Gaussian represents the RC stars and the other terms represent the red giants in the region. A nonlinear least-squares method is used to fit the profile and to obtain the parameters. The color and magnitude distributions along with the fitted profiles of a sub-region in the SMC are shown in the lower left panels of Figures 2 and 3, respectively. The parameters obtained are the coefficients of each term in the function used to fit the profile, error in the estimate of each parameter, and reduced χ^2 value. For all the sub-regions we estimated the peaks and the widths in the *I* mag and $(V-I)$ mag of the distributions, associated errors with the parameters, and reduced χ^2 values. The errors associated with the parameters are obtained using the covariance matrix, where the square root of the diagonal elements of the matrix gives the error values.

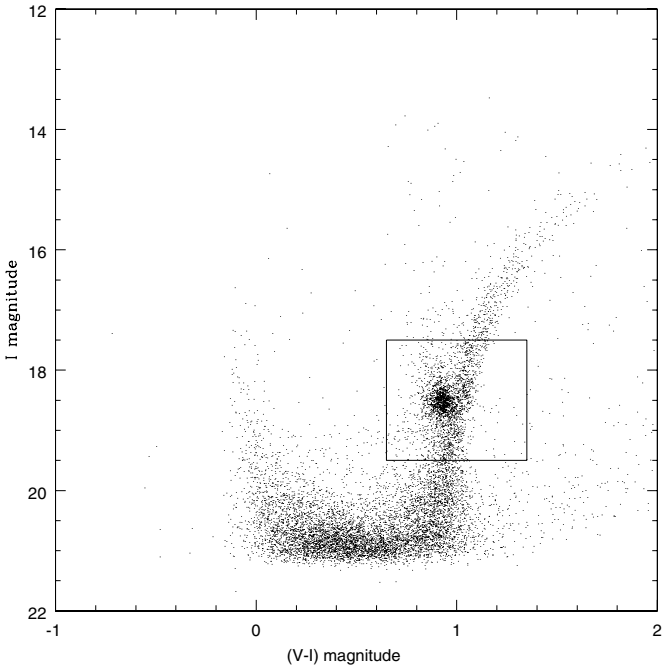

Figure 1. Color–magnitude diagram of a sub-region in the SMC. The box used to identify the red clump stars is also shown.

The number of RC stars identified within the box in the CMD is less (100–400) for 602 sub-regions. These sub-regions are located toward the edge of the survey and in the three isolated fields in the northwestern region of the SMC. For these 602 sub-regions we carefully analyzed the magnitude and color distributions. Because of the low number of stars the peaks of the distributions were not very clear and unique. It was difficult to fit those distributions with the profiles. As our methodology depends very much on the statistical analysis of the sample, we omitted these 602 sub-regions with RC stars less than 400 for the remaining analysis. Thus the number of regions used for the study reduced to 678. The magnitude and color distributions of most of these 678 regions were checked manually and we found that the fits are satisfactory.

The reduced χ^2 values and the fit errors of the peak and width of color and magnitude distributions are plotted against R.A. in the lower right, upper right, and upper left panels of Figures 2 and 3, respectively. The sub-regions with reduced χ^2 values greater than 2.0 for both magnitude and color distributions are omitted from the analysis. The regions with peak and width error greater than 0.05 mag in the magnitude distributions are also removed from the analysis. In the case of color distribution, regions with peak and width errors greater than 0.02 mag are

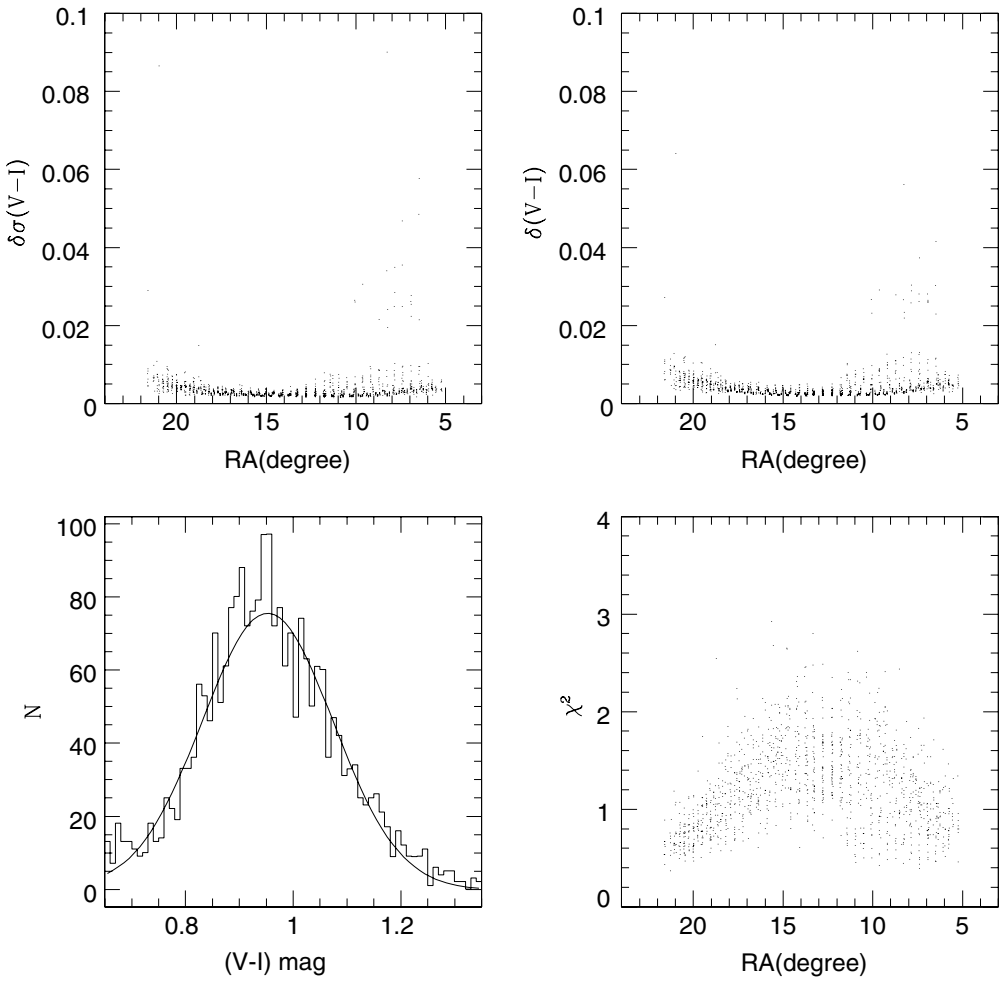

Figure 2. Typical color distribution of a sub-region is shown in the lower left panel. The best fit to the distribution is also shown. The reduced χ^2 values and the fit errors in the peak and width of the color distribution of all sub-regions are plotted against R.A. in the lower right, upper right, and upper left panels, respectively.

not considered for the analysis. Thus we used only 553 out of 678 sub-regions for the final analysis.

The peak value of the color $(V-I)$ mag at each location is used to estimate the reddening. The reddening is calculated using the relation $E(V-I) = (V-I)_{\rm obs}$–0.89 mag. The intrinsic color of the RC stars in the SMC is chosen as 0.89 mag to produce a median reddening equal to that measured by Schlegel et al. (1998) toward the SMC. The interstellar extinction is estimated by $A_I = 1.4 \times E(V-I)$ (Subramaniam 2005). After correcting the mean I mag for interstellar extinction, I_0 mag for each region is estimated.

The variation in the I_0 mag between the sub-regions is assumed only due to the difference in the relative distances. The difference in I_0 mag is converted into relative distance, ΔD using the distance modulus formula,

$$(I_0 \text{ mean } - I_0 \text{ of each region}) = 5\log_{10}(D_0/(D_0 \pm \Delta D),$$

where D_0 is the mean distance to the SMC which is taken as 60 kpc. The average error in I_0 is calculated using the formula, $\delta {I_0}^2 = (\text{avg error in peak I})^2 + (1.4 \times \text{avg error in peak } (V-I))^2$, and the error is estimated as 0.013 mag which corresponds to $\sim$360 pc.

The Cartesian coordinates corresponding to each sub-region can be obtained using the R.A., decl., and ΔD. The x-axis is antiparallel to the R.A. axis, the y-axis is parallel to the declination axis, and the z-axis is toward the observer. The origin of the system is the centroid of our sample. The centroid estimated as the mean R.A. and decl. of the final sample of the RC stars in the 553 sub-regions of the SMC is $\alpha = 0^{\rm h}52^{\rm m}34\overset{\rm s}{.}2$, $\delta = -73^\circ 2' 48''$. The x, y, and z coordinates are obtained using the transformation equations given below (van der Marel & Cioni 2001, see also the Appendix of Weinberg & Nikolaev 2001; a similar transformation for the LMC is given in Subramanian & Subramaniam 2010):

$$x = -D\sin(\alpha-\alpha_0)\cos\delta,$$

$$y = D\sin\delta\cos\delta_0 - D\sin\delta_0\cos(\alpha-\alpha_0)\cos\delta,$$

$$z = D_0 - D\sin\delta\sin\delta_0 - D\cos\delta_0\cos(\alpha-\alpha_0)\cos\delta,$$

where D_0 is the distance to the SMC and D, the distance to each sub-region, is given by $D = D_0 \pm \Delta D$. The (α, δ) and (α_0, δ_0) represent the R.A. and decl. of each sub-region and the centroid of the sample, respectively.

The estimated dispersions of the color and magnitude distributions are used to obtain the line-of-sight depth of each region in the SMC. The total width of the Gaussian in the distribution of color is due to internal reddening apart from observational error and population effects. The width in the distribution of magnitude is due to population effects, observational error, internal

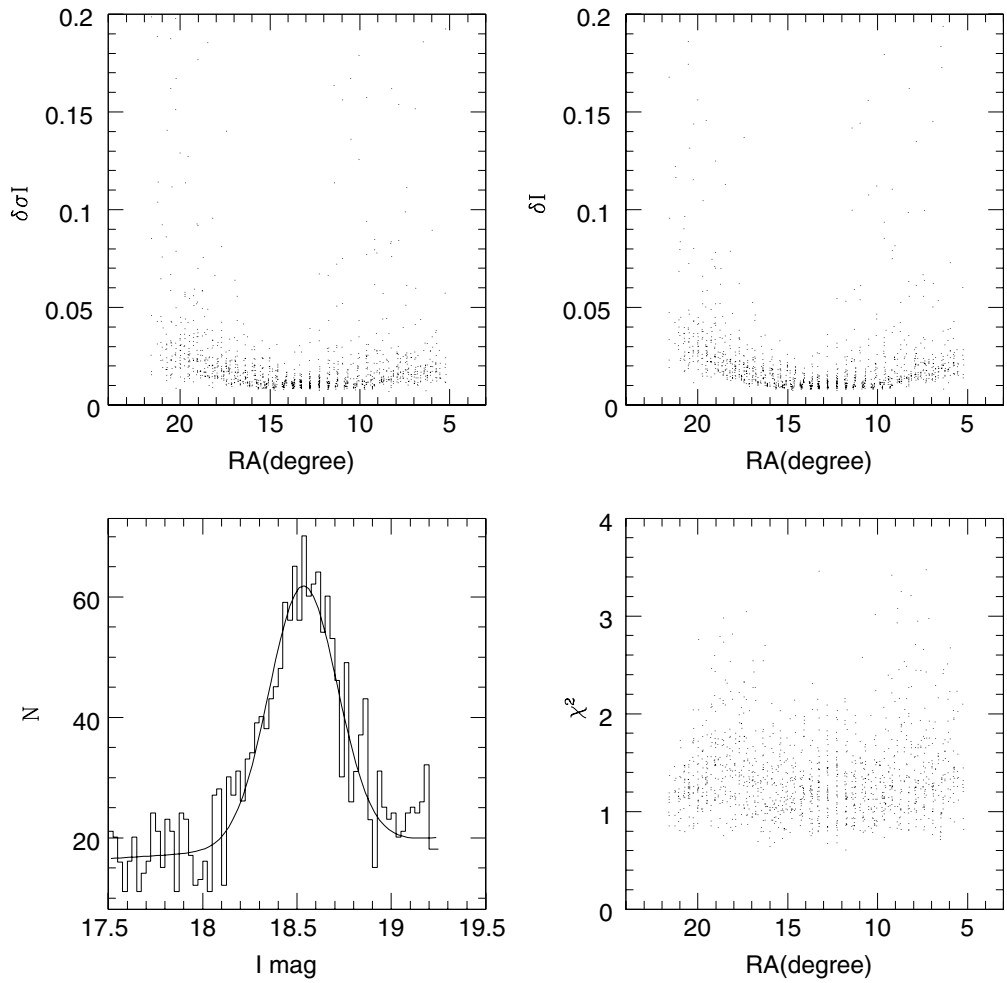

Figure 3. Typical magnitude distribution of a sub-region is shown in the lower left panel. The best fit to the distribution is also shown. The reduced χ^2 values and the fit errors in the peak and width of the magnitude distribution of all the sub-regions are plotted against R.A. in the lower right, upper right, and upper left panels, respectively.

extinction, and depth. By deconvolving the effects of observational error, extinction, and population effects from the distribution of magnitude, an estimate of the depth can be obtained. The contribution due to population effects on the observed dispersions discussed in Section 2 is corrected using the model predicted values given by Girardi & Salaris (2001). This analysis for the estimation of the depth is similar to that performed by Subramanian & Subramaniam (2009) for the OGLE II and the Magellanic Cloud Photometric Survey regions of the SMC:

$$\sigma^2_{\rm col} = \sigma^2_{\rm internal-reddening} + \sigma^2_{\rm intrinsic} + \sigma^2_{\rm error}$$

$$\sigma_{\rm internal-extinction} = 1.4 \times \sigma_{\rm internal-reddening}$$

$$\sigma^2_{\rm mag} = \sigma^2_{\rm depth} + \sigma^2_{\rm internal-extinction} + \sigma^2_{\rm intrinsic} + \sigma^2_{\rm error}.$$

Thus the width corresponding to the depth of the RC distribution in each sub-region is estimated. The error in the depth estimate which has contributions from the error in the widths of magnitude and color is also calculated. The average error in the depth estimate is ∼400 pc.

3.2. RR Lyrae Stars

A catalog of the SMC RRLS from the OGLE III survey is presented by Soszyñski et al. (2010). To study the old stellar population in the SMC, we used 1933 fundamental mode RRLS present in the catalog. We removed 29 out of 1933 stars that are brighter than the SMC RRLS and are possible Galactic objects.

The ab-type RRLS can be considered to belong to a similar class and hence can be assumed to have similar properties. The mean magnitude of these stars in the I band, after correcting for extinction effects, can be used for to estimate distance, and the observed dispersion in their mean magnitude is a measure of the depth in their distribution. The reddening obtained using the RC stars (described in the previous sub-section) is used to estimate the extinction for individual RRLS. Stars within each bin of the reddening map are assigned a single reddening and it is assumed that reddening does not vary much within the bin. Thus the extinction corrected I_0 magnitudes for all the RRLS are estimated. As in the case of the RC stars, the difference in I_0 between each RRLS is assumed to be due only to the variation in their distances and the relative distance, ΔD, corresponding to each star is estimated. The error in the relative distance estimation of individual RRLS is basically the error in the extinction correction of I_0 mag. The average error in the extinction estimation, obtained from the RC stars, converts to a distance of ∼110 pc. The location of each RRLS in the Cartesian coordinate system is then calculated using the transformation equations given in the previous section.

Using the dereddened I_0 magnitude of each RRLS, the dispersion in the surveyed region of the SMC can be found. The

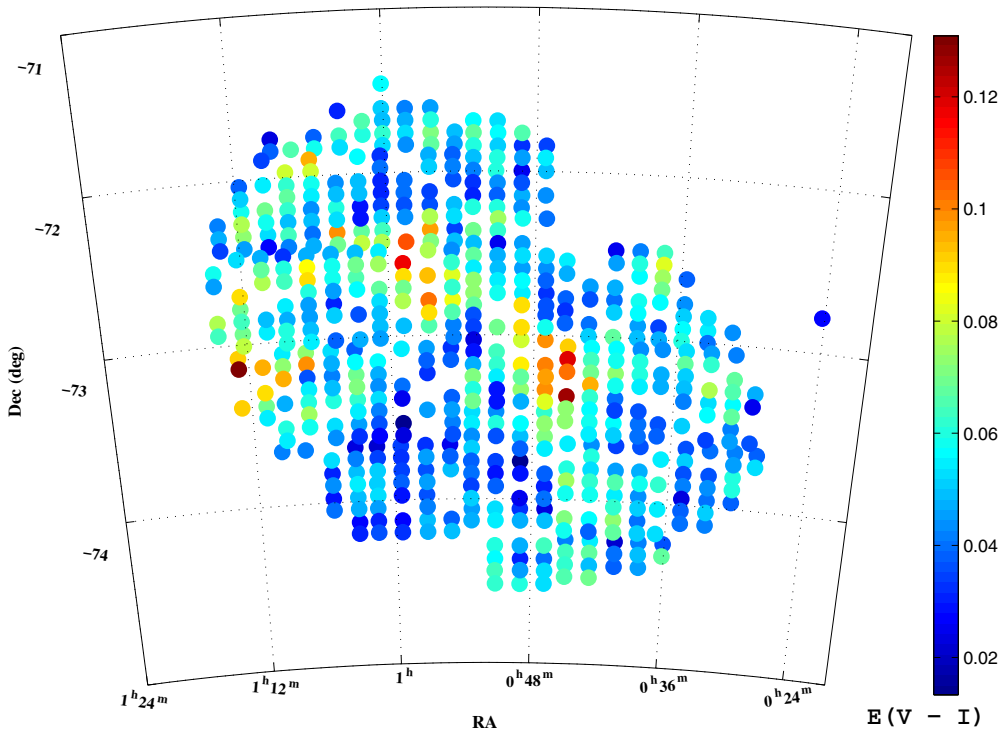

Figure 4. Two-dimensional plot of the reddening in the sub-regions of the SMC.
(A color version of this figure is available in the online journal.)

dispersion is a measure of the depth of the SMC. The data are binned in 0.°5 in both x- and y-axes to estimate dispersion. Thus the observed region is divided into bins with an area of 0.25 deg^2. The number of stars in each bin has a range of 10–50. The bins with stars less than 10 are removed from our analysis. For each location we estimated the mean magnitude and the dispersion. The estimated dispersion has contributions from photometric errors, range in the metallicity of stars, intrinsic variation in the luminosity due to evolutionary effects within the sample, and the actual depth in the distribution of the stars (Clementini et al. 2003). We need to remove the contribution from the first three terms ($\sigma_{\rm intrinsic}$) so that the value of the last term can be evaluated. Clementini et al. (2003) estimated a value of $\sigma_{\rm intrinsic}$ as 0.1 mag for their sample of 100 RRLS in the LMC. Subramaniam (2006) used a larger sample of RRLS in the LMC from the OGLE II catalog and estimated the value of $\sigma_{\rm intrinsic}$ as 0.15 mag. Both of these values are estimated using the globular cluster data in the observed field. In the case of the SMC, there is only one globular cluster and it is not in our observed field, so we used the intrinsic spread estimated for the RRLS in the LMC for the analysis of the RRLS in the SMC. Using both these values we estimated the corrected σ values which correspond only to depth. The relation used is

$$\sigma^2_{I_0{\rm mag}} = \sigma^2_{\rm depth} + \sigma^2_{\rm intrinsic}.$$

4. REDDENING MAP OF THE SMC

One of the by-products of this study is the estimation of reddening toward the SMC. The observed shift of the peak $(V-I)$ color of the RC stars in the LMC from the expected value was used by Subramaniam (2005) to estimate the line-of-sight reddening map to the OGLE II regions of the LMC. Such a reddening map toward the SMC using the RC stars is obtained here. The intrinsic value of the $(V-I)$ color of the RC stars in the SMC is chosen as 0.89 mag to produce a median reddening equal to that measured by Schlegel et al. (1998) toward the SMC. Using this value the $E(V-I)$ values are estimated as detailed in Section 3.1. The color-coded figure of the reddening in the SMC is presented in Figure 4. The color code is given in the plot. The average value of $E(V-I)$ obtained toward the SMC is 0.053 ± 0.017 mag. From the plot we can see that most of the regions in the SMC have $E(V-I)$ less than 0.08 mag shown as cyan and blue points. The regions in the southwestern and northeastern sides of the center and the eastern wing regions have larger reddening compared to the other regions of the SMC. This reddening map estimated using the RC stars is used to deredden the RC stars as well as the RRLS in this study. These reddening data will be made available electronically as an online table.

Previous estimates of the reddening toward the SMC are compared with ours. Caldwell & Coulson (1985) found a mean $E(B-V)$ of 0.054 mag from the analysis of 48 Cepheids. This value can be converted into an $E(V-I)$ of 0.0756 mag using the relation $E(V-I) = 1.4 \times E(B-V)$ (Subramaniam 2005). Udalski (1998) (using RC stars) estimated a mean $E(V-I)$ value of 0.1 mag. Massey et al. (1995) and Grieve & Madore (1986) estimated an $E(B-V)$ of around 0.09 mag which converts to an $E(V-I)$ value of 0.126 mag. Haschke et al. (2011) provided the reddening maps toward the SMC from the study of the RC stars and RRLS. The intrinsic color of the RC stars used by them is also 0.89 mag. The reddening map of the SMC estimated from the RC stars given in Figure 4 of Haschke et al. (2011) is very similar to our reddening map given in Figure 4. The mean value of $E(V-I)$ estimated by them toward the SMC using the RC stars is 0.04 mag and that estimated from RRLS is 0.07 mag. The reddening maps of the RC stars and RRLS given in Figures 4 and 11 of Haschke

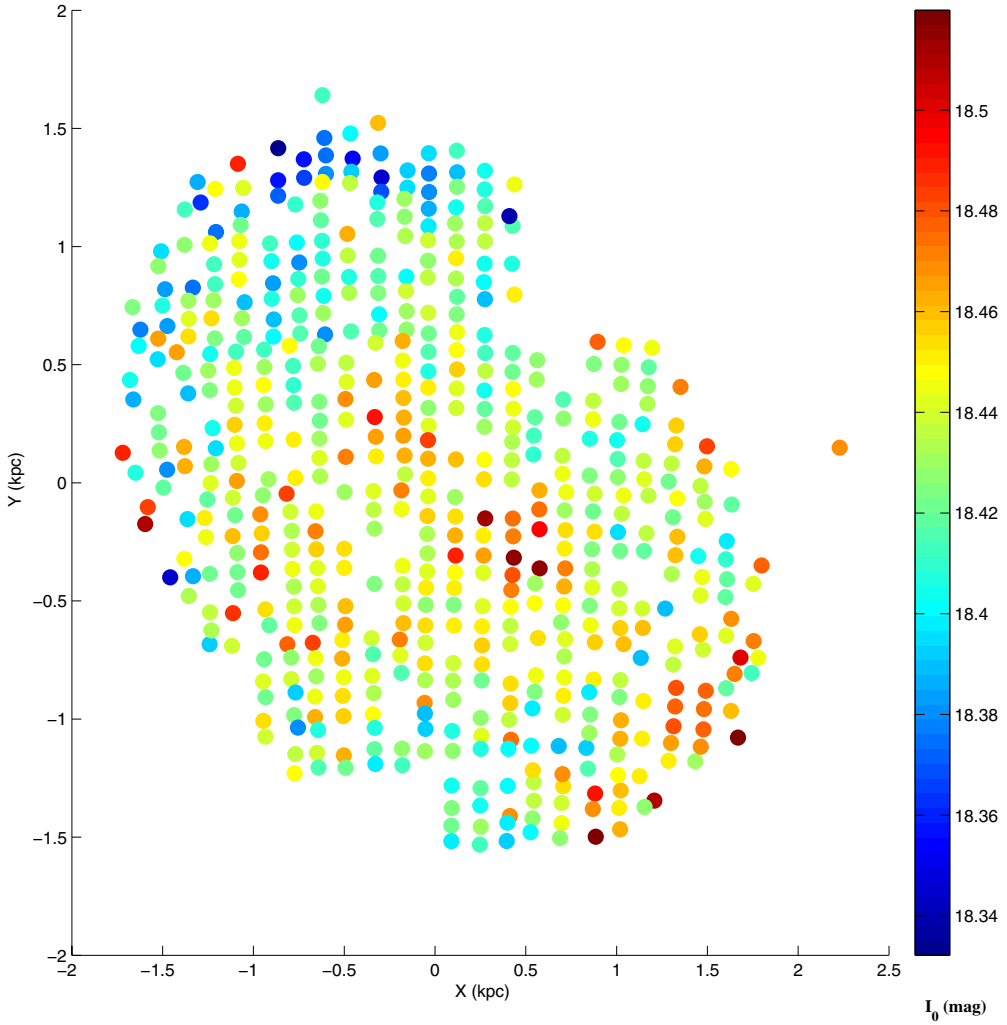

Figure 5. Two-dimensional plot of the mean magnitudes of the RC stars in the sub-regions of the SMC.
(A color version of this figure is available in the online journal.)

et al. (2011) are very similar. This fact supports and validates our usage of the reddening map obtained from the RC stars to deredden the RRLS. Previous estimates aside from those of Haschke et al. (2011) are higher than ours. This could be due to the choice of our intrinsic $(V-I)$ color of the RC stars in the SMC, but such a change will only shift the reddening value in all regions in a similar way. As we are only interested in the relative positions of the regions in the SMC, such a change in the intrinsic color of the RC stars is not going to affect our final results.

In order to compare the adopted intrinsic color of the RC stars in the SMC with theoretical values, we measured the peak color of the RC stars from the synthetic CMD of the SMC given in Girardi & Salaris (2001). It turned out to be ∼0.89 mag. The table given in Girardi & Salaris (2001) provides an RC $(V-I)_0$ color for the LMC metallicity of $z = 0.004$ between 0.90 and 0.94 mag (age between 2 and 9 Gyr). For a lower metallicity of $z = 0.001$, their models lead to a color between 0.8 mag and 0.84 mag (age between 2 and 9 Gyr). The mean metallicity found by Cole (1998) and Glatt et al. (2008) for the SMC is between 0.002 and 0.003. This value supports our adopted value of $(V-I)_0$ color for the RC stars in the SMC, which is bluer than that of the LMC and redder than the color obtained for a lower metallicity system.

5. RESULTS

5.1. Relative Distances

The mean dereddened I_0 magnitudes of the RC stars for the 553 sub-regions of the SMC are estimated. The mean magnitudes of different sub-regions are shown as different color points in the two-dimensional plot of X versus Y in Figure 5. The color code is given in the figure. The average dereddened magnitude I_0 of the 553 sub-regions is 18.43 ± 0.03 mag. The regions in the south ($y < 0$) are fainter compared to the regions in the north. The brighter regions ($I_0 < 18.39$) shown as blue points are located more in the northeastern side. This result indicates that the northeastern regions of the SMC are closer to us.

The relative distance to each RRLS with respect to the mean distance to the SMC is estimated from the dereddened I_0 magnitude, assuming that the average distance to our sample of RRLS in the SMC is 60 kpc. The spatial distribution of RRLS in the XZ and YZ planes with overplotted density contours is shown in Figures 6 and 7, respectively. The convention of the +ve and −ve Z-axes is such that the +ve Z-axis is toward us and the −ve Z-axis is away from us. The distribution of RRLS in the SMC looks more or less symmetric and extends from −20 kpc to +20 kpc with respect to the mean. Most of the stars are located between ±10 kpc. An extension to large distances

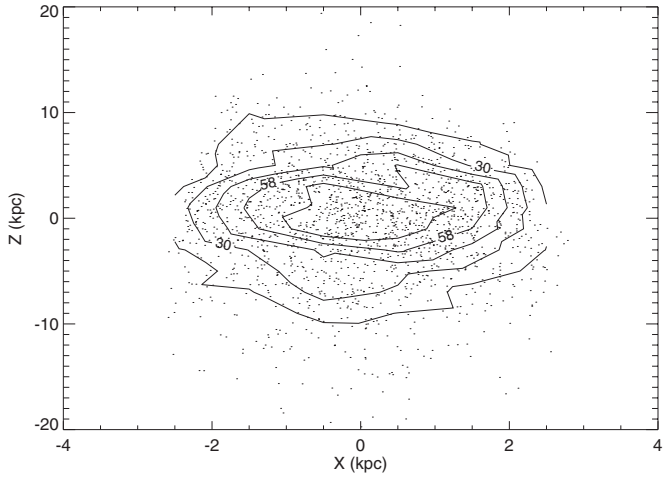

Figure 6. Relative distances to each RR Lyrae star in the SMC with respect to the mean distance are plotted against the *X*-axis and are shown as black dots. The density contours are overplotted. East is in the direction of decreasing *X*-axis.

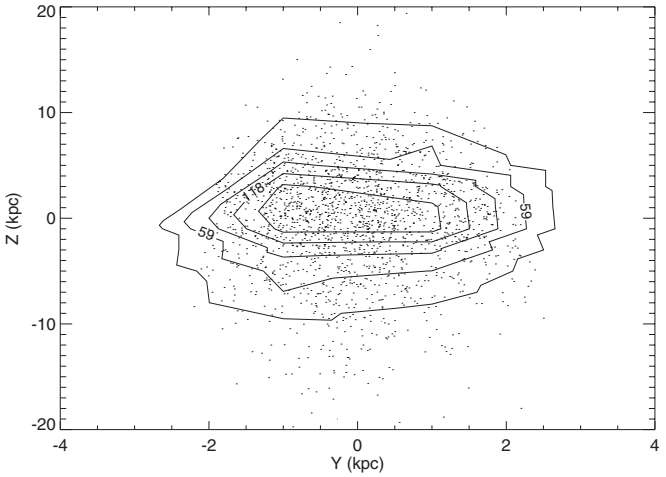

Figure 7. Relative distances to each RR Lyrae star in the SMC with respect to the mean distance are plotted against the *Y*-axis and are shown as black dots. The density contours are overplotted. North is in the direction of increasing *Y*-axis.

can be seen at $x \sim 0$. The outer density contours shown in Figure 6 indicate that the eastern side of the SMC is on average closer to us than the western side. We calculated the average I_0 magnitude of RRLS in the eastern end ($x < -1.5$, 245 stars) and in the western end ($x > 1.5$, 221 stars). It was found that the eastern side is 0.034 mag brighter than the western side, which makes the eastern side on average 950 pc closer to us than the western side. Similarly, the outer density contours shown in Figure 7 suggest that the northern side is closer to us than the southern side. We calculated the average I_0 in the northern end ($y > 1.5$, 133 stars) and in the southern end ($y < -1.5$, 104 stars). It was found that the northern side is 0.019 mag brighter than the southern side, which makes the northern side on average 520 pc closer to us than the southern side. Thus the outer density contours of Figures 6 and 7 and the quantitative estimates mildly suggest that the northeastern part of the SMC is closer to us. This result is very similar to the result obtained from the RC stars. As this effect is significant in the outer regions and our study is limited to the inner regions, we need more data in the outer regions to securely say that the northeastern part of the SMC is closer to us. From the photometric study of stellar populations up to 11.1 kpc in the SMC, Nidever et al. (2011) found that the eastern part of the SMC is closer to us than the western side.

In the case of the RC stars as well as RRLS, the variation in the I_0 magnitude is assumed to be due only to the difference in the distances. As discussed earlier in Section 2, there can be contributions in their mean magnitude from the population effects. Thus the line-of-sight distance estimates suggest that either the RC star and RRLS in the northeastern part of the SMC are different from those found in the other regions of the SMC and/or the northeastern regions of the SMC are closer to us. The previous studies mentioned in Section 2 suggest that there is no large variation in the age and metallicity among old stars in the inner SMC. Thus the contribution to the I_0 magnitude from the population effects across the SMC is expected to be minimum. The exact contribution can be understood only from the detailed spectroscopic studies of the old stellar populations.

5.2. Line-of-sight Depth of the SMC

The dispersions in the magnitude and color distributions of the RC stars are used to obtain the depth corresponding to the width (1σ) of the 553 sub-regions in the SMC. The width corresponding to depth is converted into depth in kiloparsecs using the distance modulus formula,

$$\sigma_{\rm depth} = 5 \log_{10}[(d_0 + d/2)/(d_0 - d/2),$$

where d is the line-of-sight depth in kiloparsecs.

A color-coded, two-dimensional plot of depth is shown in Figure 8. The color code is explained in the plot. From the plot we can see that the depth distribution in the SMC is more or less uniform. The prominent feature in the plot is the enhanced depth (depth >8 kpc) seen near the central regions. An increased depth of around 6–8 kpc is also seen near the northeastern regions. The average depth obtained for the SMC observed region is 4.57 ± 1.03 kpc. These results match well with the previous depth estimates by Subramanian & Subramaniam (2009).

The dispersion in the mean magnitude of RRab stars is also used to estimate the depth (1σ) of the SMC. The dispersion in the mean magnitude for 70 sub-regions of the SMC is estimated and converted into depth in kiloparsecs. The average value of depth estimated when the intrinsic spread was taken as 0.1 mag is 4.07 ± 1.68 kpc and the average depth is 3.43 ± 1.82 kpc when 0.15 mag was taken as the intrinsic spread. These estimates match with the depth estimate obtained from the RC stars within the error bars.

The depths estimated using the RC stars and RRLS are plotted together in Figure 9 against the *X*- and *Y*-axes. In both of the lower panels, the depth values are plotted against the *X*-axis and in both of the upper panels, they are plotted against the *Y*-axis. Basically, the depth values correspond to the extent (front to back distance) over which these stars are distributed in the SMC. The measured 1σ depth (front to back distance) is halved and plotted along the +ve and −ve depth axis, assuming that the depth is symmetric with respect to the SMC. The red crosses correspond to the depth estimated using the RC stars and the black points correspond to the depth estimated using the RRLS. The error bars for each point are not plotted to avoid crowding. In the left panels, the black dots correspond to the depth estimated using the RRLS when the $\sigma_{\rm intrinsic}$ is taken as 0.1 mag. Similarly, in the right panels the black dots correspond to the depth estimated using the RRLS when the $\sigma_{\rm intrinsic}$ is taken as 0.15 mag. The larger depth near the center ($x \sim 0$ and $y \sim 0$) is seen for both populations. The 18 regions in the right panels and the

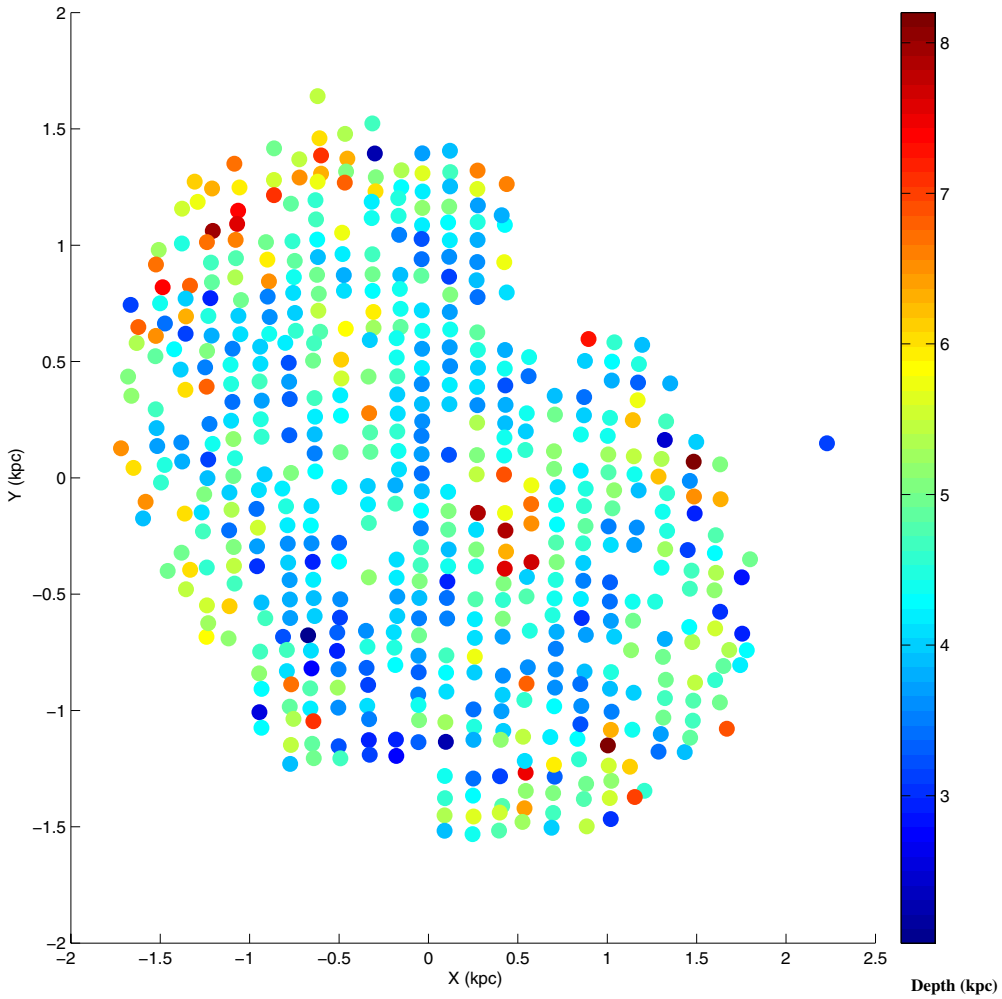

Figure 8. Two-dimensional plot of the depth in the sub-regions of the SMC obtained from the analysis of the RC stars.
(A color version of this figure is available in the online journal.)

3 regions in the left panels which are shown as open circles at zero depth are those for which the depth of the RRLS became less than zero when the correction for $\sigma_{\rm intrinsic}$ was applied. For a large number of regions the depth value becomes less than zero when $\sigma_{\rm intrinsic}$ is taken as 0.15 mag. Thus, it appears to be more appropriate to take $\sigma_{\rm intrinsic}$ as 0.1 mag for the RRLS in the SMC. The depth profiles of both populations are similar, suggesting that both the RC stars and RRLS occupy a similar volume in the SMC.

It is important to see how the dispersion in the distribution of the RRLS is related to the real RRLS distribution, obtained from the individual RRLS distances. This comparison will help us to estimate the actual depth from the dispersion of the RRLS in the SMC. We halved the 1σ depth (front to back distance estimated after correcting for $\sigma_{\rm intrinsic}$ to be taken as 0.1 mag) obtained for each sub-region with respect to the mean distance and plotted in the $-$ve and +ve Z-axis as open circles against the X-axis in the lower left panel of Figure 10. Similarly, 2σ depth, 3σ depth, and 3.5σ depth are plotted in the lower right panel, upper right panel, and upper left panel of Figure 10, respectively. The individual RRLS distances with respect to the mean SMC distance are shown as black dots in all the panels of Figure 10. From the figure we can clearly see that the distribution of RRLS is at least extended up to 3.5σ dispersion, if we take an intrinsic spread of 0.1 mag. This 3.5σ width ($\sigma_{\rm dep} = 0.146$ mag) translates to a front to back distance of around 14.12 kpc. In Figure 11, the depth estimated from RRLS after correcting for $\sigma_{\rm intrinsic} = 0.15$ mag is plotted over the individual RRLS distances. The upper left panel shows the 4σ depth plotted over the individual RRLS distances. From the figure we can clearly see that the distribution of RRLS is at least extended to 4σ dispersion, if we take an intrinsic spread of 0.15 mag. This 4σ width ($\sigma_{\rm dep} = 0.124$ mag) translates into a front to back distance of around 13.7 kpc. Thus the RRLS in the SMC are distributed over a distance of $\sim$14 kpc along the line of sight. In the case of the RC stars, we have estimated only the mean distances to the sub-regions and the depth of the sub-regions, so we cannot compare the real RC distribution with the width of the distribution to define the depth. Since the depth profiles of the RC stars and the RRLS are similar, we expect these two populations to occupy a similar volume in the SMC and the RC stars also to be distributed in a depth of 14 kpc. The large depth suggests a spheroidal/ellipsoidal distribution for the above populations.

5.3. Density Distributions of RC and RR Lyrae Stars

From the above section, we found that both the RC stars and RRLS have similar line-of-sight depth. The density distributions of both these populations will give a clue about the system in the XY plane. The surface density distribution and the radial density

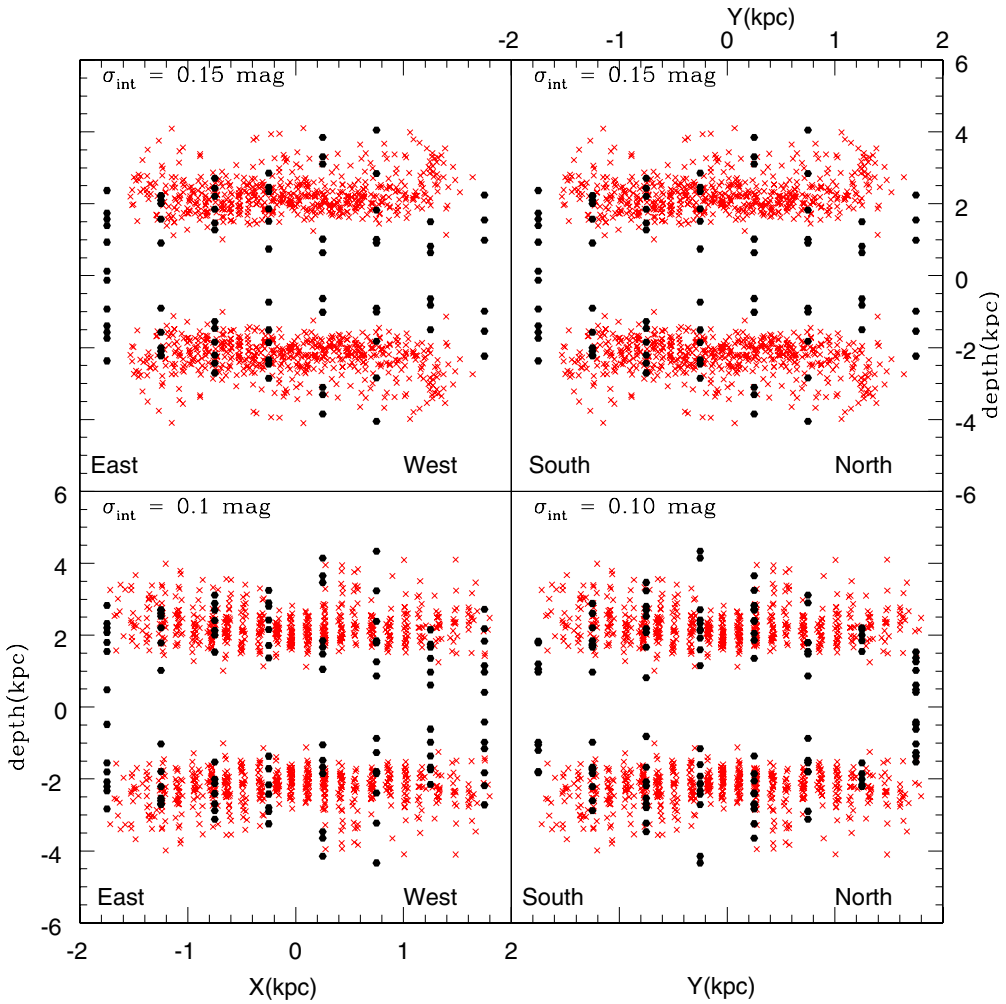

Figure 9. Line-of-sight depth (1σ) of both the RC stars (red crosses) and the RRLS (black dots) are plotted against the X- and Y-axes. In the lower left and upper left panels, the RRLS depth estimates are given using $\sigma_{\rm intrinsic} = 0.1$ mag. In the lower right and upper left panels, the RRLS depth estimates are done using $\sigma_{\rm intrinsic} = 0.15$ mag.

(A color version of this figure is available in the online journal.)

profile are studied to understand the structure of the SMC. The surface density is calculated by dividing the observed region into different sub-regions and obtaining the number of objects per unit area in each sub-region. The radial density profiles are obtained by finding the projected radial number density of objects in concentric rings around the centroid of the SMC. These profiles can be compared with the theoretical models. The two theoretical models which can be used for the comparison of spatial distribution of different stellar populations in the SMC are the exponential disk profile and the King's profile. The exponential disk profile is given by

$$f(r) = f_{0d} \mathrm{e}^{-r/h},$$

where f_{0d} and the h represent the central density of the objects and the scale length, respectively, and r is the distance from the center of the distribution. The King's profile (King 1962), which is often used to describe the distribution of globular clusters, but also applies to dwarf spheroidal galaxies, is given by

$$f(r) = f_{0k}\{[1 + (r/a)^2]^{-1/2} - [1 + (r_t/a)^2]^{-1/2}\}^2,$$

where r_t and a are the tidal and core radii, respectively, f_{0k} is the central density of objects, and r is the distance from the center. Both these profiles are used to fit the observed distribution of the RC stars in the SMC.

The number of RC stars, identified from the CMD, in each sub-region of the OGLE III region is estimated. We used all 1280 sub-regions (each having an area of 32.6 kpc^2) in the observed OGLE III region. We estimated the number density, number of the RC stars per unit area, for each sub-region. The number density distribution of the RC stars is shown in Figure 12. The number density of RC stars in each sub-region ranges from 7500 kpc^{-2} to 200,000 kpc^{-2}. In this figure, discrete points represent each sub-region and the color denotes the number density. The plot clearly shows the smooth RC distribution with an elongation in the northeast to southwest (NE–SW) direction. The color code is given in the figure, where d denotes the RC number density. The position angle of the elongation of the RC distribution is around 54° for the eastern side. The plot also shows the shift in the RC density center, $\alpha = 0^{\rm h}52^{\rm m}34\overset{\rm s}{.}2$, $\delta = -73^\circ 2' 48''$ (shown as green hexagons in Figure 12) from the optical center, $\alpha = 0^{\rm h}52^{\rm m}45^{\rm s}$, $\delta = -72^\circ 49' 43''$ (shown as magenta hexagons in Figure 12) of the SMC. The center of the density distribution shown here is very similar to the centroid (given in Section 3.1) of our RC sample in 553 sub-regions which are used for the estimation of dereddened magnitude and depth.

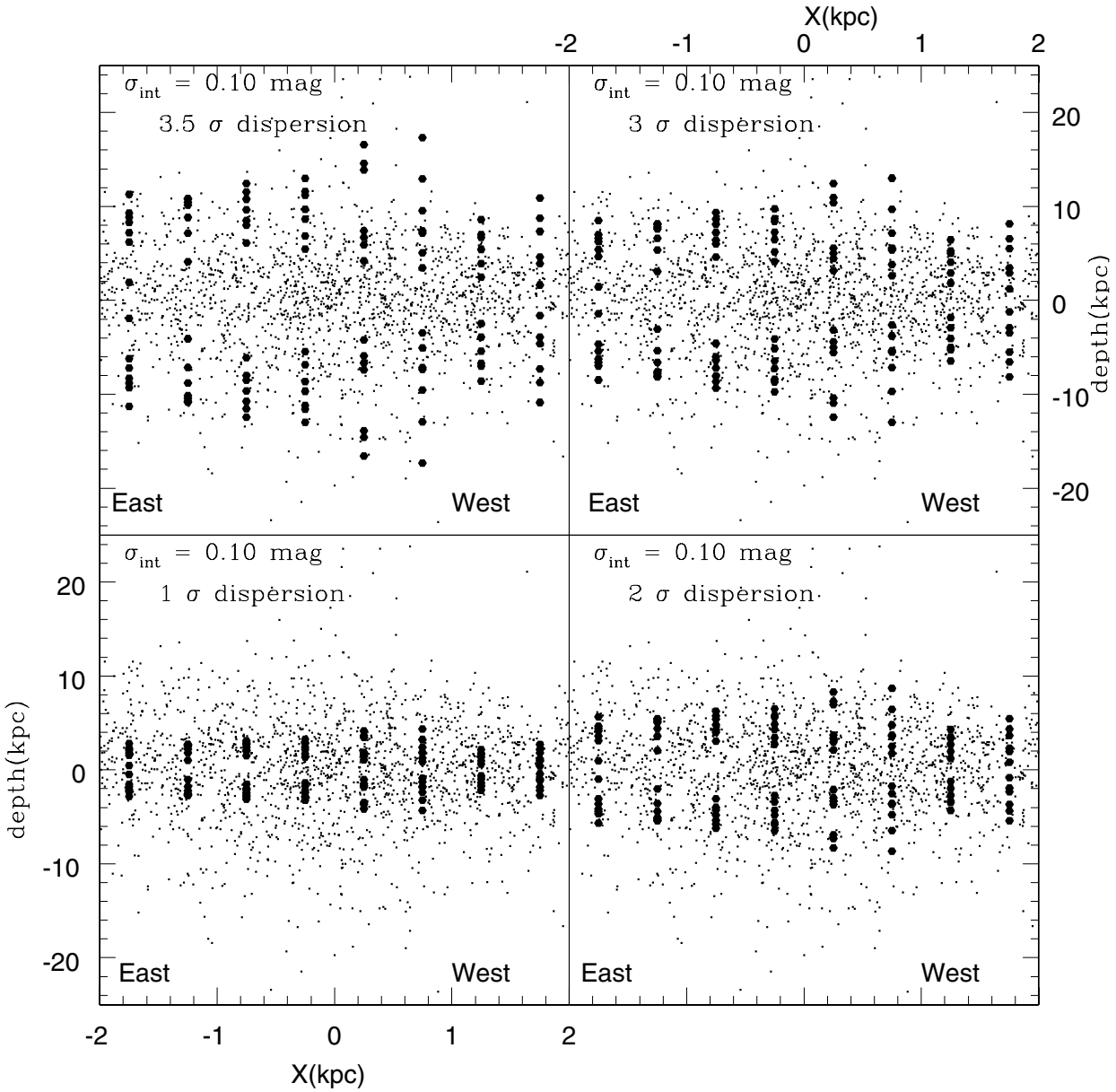

Figure 10. Distance to each RRLS with respect to the mean distance to the SMC is plotted as black dots in all the panels against the *X*-axis. The open circles in all the panels from lower right to upper left in counterclockwise direction are the 1σ, 2σ, 3σ, and 3.5σ depths halved with respect to the mean distance to each sub-region and plotted in the −ve and +ve *Z*-axis against the *X*-axis. The depth is calculated using an intrinsic spread of 0.1 mag.

As the data coverage of the OGLE III is not symmetric with respect to the density center, the radial density distribution of the RC stars within a radius of 0.°8 is obtained. The region within a 0.°8 radius from the density center is divided into 16 equal area (28.3 arcmin^2) annuli. The number of RC stars in each annuli is obtained and it is divided by the area of the annuli to obtain the number density. Thus the radial density distribution of the RC stars within a 0.°8 radius from the density center is obtained and is shown as black squares in Figure 13. The best-fitted exponential disk profile and the King's profile are shown in the figure as green and blue solid lines, respectively. We can see that the radial density profile of the RC stars in the SMC is described marginally better by the King's profile than by the exponential profile. We obtained the surface density profile of the RC stars in the whole observed area of the SMC. The number density of the RC stars in the 1280 sub-regions of the SMC is plotted against the radial distance of each sub-region from the density center in Figure 13. The black points in the figure denote the surface density of the RC stars in each sub-region. The best-fit exponential disk profile and the King's profile are shown as green and blue dashed lines, respectively, in Figure 13. Here we can see that the surface density profile of the RC stars in the SMC is best described by the King's profile. The parameters obtained by fitting the radial density and surface density distributions by exponential and King's profiles are given in Table 1. The estimated tidal radius of the SMC system is ∼7–12 kpc. Thus the RC stars in the SMC are distributed in a spherical/ellipsoidal volume, which indicates that the SMC can be approximated as a spheroidal/ellipsoidal galaxy, but in the surface density profile we can see a spread in the points for each radii, which indicates that the volume in which the RC stars are distributed is not exactly spherical. Again, from the map of the surface density distribution shown in Figure 12, we can see the elongation in the NE–SW direction. Thus the RC stars in the SMC are distributed in an ellipsoidal system.

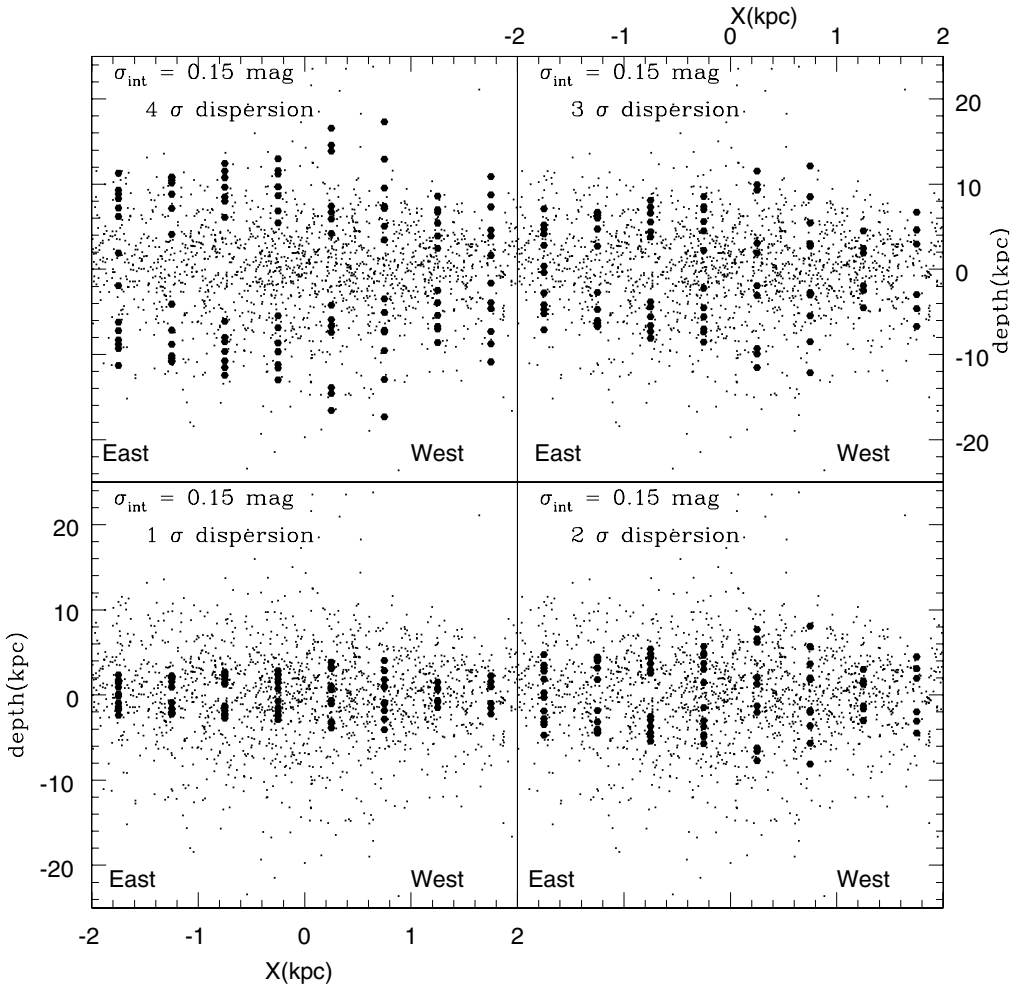

Figure 11. Distance to each RRLS with respect to the mean distance to the SMC is plotted as black dots in all the panels against the *X*-axis. The open circles in all the panels from lower right to upper left in the counterclockwise direction are the 1σ, 2σ, 3σ, and 4σ depths halved with respect to the mean distance to each sub-region and plotted in the −ve and +ve *Z*-axis against the *X*-axis. The depth is calculated using an intrinsic spread of 0.15 mag.

Table 1
Parameters of the Exponential and King's Profiles

Data	f_{0d} (no kpc^{-2})	h (kpc)	f_{0k} (no kpc^{-2})	r_c (kpc)	r_t (kpc)
Radial density distribution	$(104 \pm 0.4) \times 10^3$	1.87 ± 0.1	$(141 \pm 7) \times 10^3$	1.08 ± 0.02	7 ± 1
Surface density distribution	$(264 \pm 0.1) \times 10^3$	0.91 ± 0.1	$(248 \pm 1) \times 10^3$	0.9 ± 0.01	12.04 ± 0.01

Our sample of RRLS that are pulsating in the fundamental mode consists of 1904 stars. The density center of our sample is $\alpha = 0^h53^m31^s$, $\delta = -72°59'15\farcs7$. The density center of our sample lies in between the two concentrations found by Soszyñski et al. (2010). To study the density profiles, a large number of samples is required. The surface density map of the RRLS identified from the OGLE III photometric maps is shown in the lower panel of Figure 7 in Soszyñski et al. (2010). They identified two concentrations in the RRLS spatial distribution and found that the RRLS in the SMC form a roughly circular structure in the sky which indicates that they are distributed in a spheroidal/ellipsoidal volume.

6. AXES RATIO AND ORIENTATION OF THE SMC ELLIPSOID

We model the observed system of the SMC in which the RC stars and RRLS are distributed as a triaxial ellipsoid. The parameters of this ellipsoidal system, like the axes ratio and the orientation, can be estimated using the inertia tensor analysis. The tensor analysis used here is similar to the methods used by Pejcha & Stanek (2009) and Paz et al. (2006), but with some modification. The tensor analysis used in the study is explained in the Appendix.

6.1. RR Lyrae Stars

The method described in the Appendix can be applied to our sample of the RRLS to estimate the parameters of the ellipsoidal component of the SMC. First, we applied this method only to the (x,y) system and found that the SMC RR Lyrae distribution is elongated with an axes ratio of 1:1.3 and the major axis has a position angle of 74° (NE–SW). We repeated the procedure for the (x, y, z) coordinates of the RRLS. The axes ratio obtained was 1:1.3:6.47 and the longest axis is inclined with the line-of-sight direction with an angle (i) of 0°.4. The position angle of the

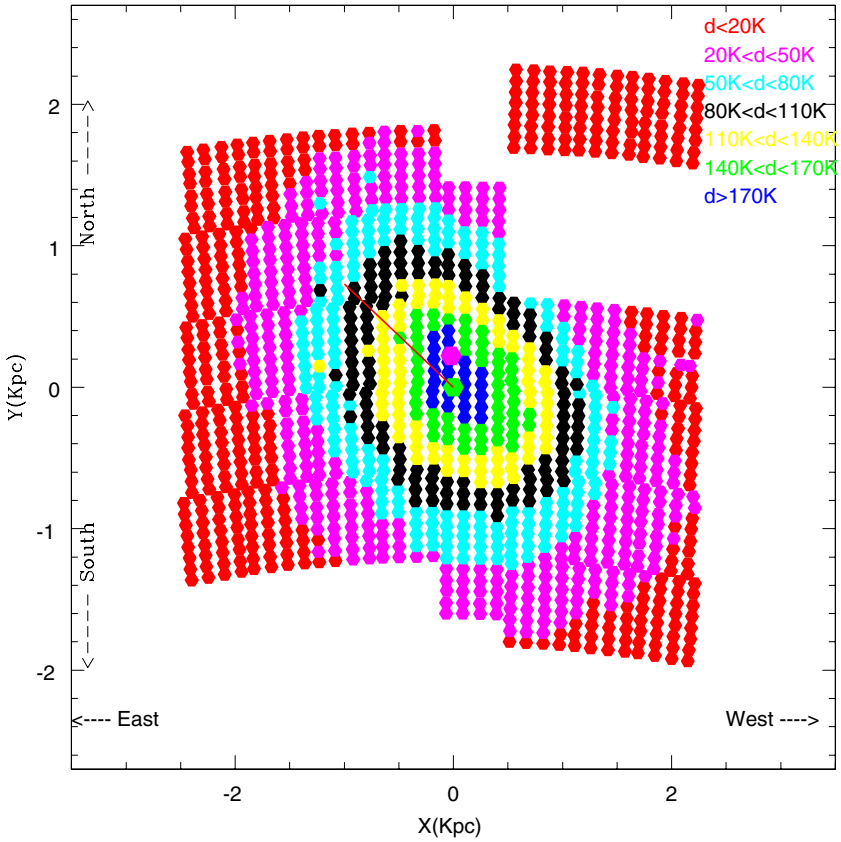

Figure 12. Two-dimensional plot of the number density, d, of the RC stars (d in the units of 1000(K) kpc^{-2}) in the SMC. The green and magenta hexagons represent the centroid of the sample and the optical center, respectively. The red line shows the direction of elongation.

(A color version of this figure is available in the online journal.)

projection of the ellipsoid (ϕ) on the plane of the sky is given by 74.°4. The data of the RRLS used here contain the RRLS in the isolated northwestern OGLE III fields. As they are discrete points in the density distribution, we removed the RRLS in those fields and repeated the procedure. When we removed the RRLS in those fields, the density center changed to $\alpha = 0^{\rm h}54^{\rm m}38.^{\rm s}6$, $\delta = -73°4'52.''2$. The axes ratio obtained is 1:1.57:7.71 with $i = 0.°4$ and $\phi = 66.°0$. Here we can see that the coverage of the data plays an important role in the estimation of the structural parameters of the ellipsoid. This may also suggest that there may be a variation in the inner and outer structures of the SMC. Nidever et al. (2011) found that the inner SMC ($R < 3°$) is more elliptical than the outer component ($3° < R < 7.°5$).

In order to understand the radial variation of the inner structure, we estimated the parameters using the data within different radii. At first, the analysis is done excluding the RRLS in the northwestern fields. The axes ratio i and ϕ of the RRLS distribution are obtained for the data within different radii, starting from 0.°75. The values obtained are given in Table 2. The values show that i is more or less constant with a value of around 0.°5, but the axes ratio and ϕ have a range of values. The axes ratio has a range from 1:1.05:19.84 to 1:1.57:7.7. ϕ ranges from 60° to 78°. The data within 0.°75 of the density center are symmetric and the parameters obtained confirm that the RRLS distribution in the SMC is slightly elongated in the NE–SW direction. As the radius increases the data coverage is not symmetric and circular, and the axis ratio of x and y shows an increasing trend. The surface density map of RRLS shown in Figure 7 of Soszyński et al. (2010) does not show large elongation; rather the map looks nearly circular with a mild elongation in the NE–SW direction. Thus the elongation obtained for the RRLS distribution in the plane of the sky, at a larger radius where the data coverage is not even, may not be real. We conducted a similar analysis to understand the radial variation including the fields in the northwestern regions. Here the concentric circles with different radii are centered on the density center (given in the last paragraph) estimated including the RRLS in the northwestern fields. These values are also given in Table 2. From this analysis it is also evident that there is a mild elongation in the NE–SW direction in the distribution of the RRLS in the SMC. Here we have to also keep in mind that the density center estimation of the SMC RRLS is not accurate as there are two concentrations found in the density distribution shown in Figure 7 of Soszyński et al. (2010). The variation in the density center also modifies the structural parameters of the distribution.

From the detailed analysis described in the last two paragraphs, it is clear that the quantitative estimates of the structural parameters of the SMC are very much dependent on the data coverage. Though there are differences in the values, we can say that the RR Lyrae distribution in the inner SMC is slightly elongated in the NE–SW direction. The longest axis Z', which is perpendicular to the $X'Y'$ plane (a plane obtained by the counterclockwise rotation of the XY plane with an angle ϕ with respect to the Z-axis), is aligned almost parallel to the line of sight Z-axis. The x, y, and z values of the whole sample of the RRLS are plotted in Figure 14 to get a three-dimensional visualization of the SMC structure. The figure clearly shows the elongation in the $Z' \sim Z$ axis.

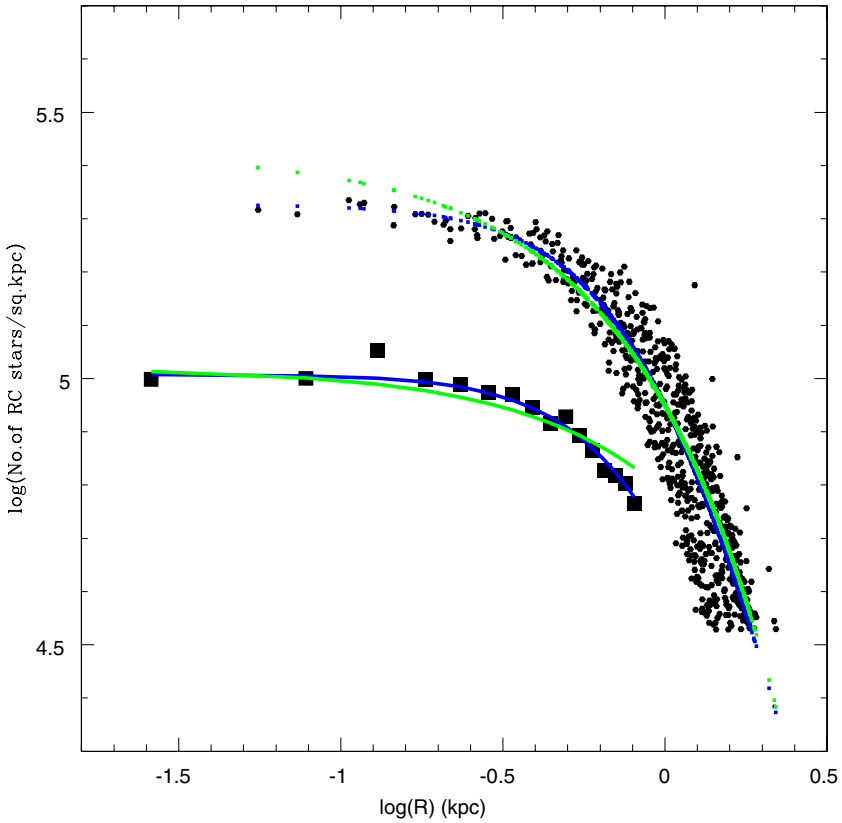

Figure 13. Radial density distribution of the RC stars within a radius of 0.°8 in the SMC is shown as black squares. The best-fit King's profile and the exponential profile for the radial density distribution are shown as blue and green solid lines, respectively. The surface density distribution of the RC stars for the whole observed region of the OGLE III is shown as black dots. The best-fit King's profile and the exponential profile for the surface density distribution are shown as blue and green dashed lines, respectively.

(A color version of this figure is available in the online journal.)

Table 2
Orientation Measurements of the Ellipsoidal Component of the SMC Estimated Using the RR Lyrae Stars

Data	No. of RRLS	Axes Ratio	i	ϕ
Excluding the three northwestern fields, Center: $\alpha = 0^{h}54^{m}38\overset{s}{.}6$, $\delta = -73°4'52\overset{''}{.}2$				
$r < 0.°75$	421	1:1.05:19.84	0.°4	78.°83
$r < 1.°00$	676	1:1.03:14.59	0.°4	72.°20
$r < 1.°25$	924	1:1.04:11.35	0.°2	75.°68
$r < 1.°50$	1187	1:1.10:9.43	0.°1	63.°41
$r < 1.°75$	1407	1:1.23:8.66	0.°1	61.°68
$r < 2.°00$	1563	1:1.34:8.21	0.°1	66.°00
$r < 2.°25$	1711	1:1.47:7.87	0.°3	67.°62
$r < 2.°50$	1780	1:1.54:7.73	0.°4	67.°48
$r < 2.°75$	1798	1:1.57:7.71	0.°4	66.°30
$r < 3.°00$	1803	1:1.57:7.71	0.°4	65.°96
Including the northwestern fields, Center: $\alpha = 0^{h}53^{m}31^{s}$, $\delta = -72°59'15\overset{''}{.}7$				
$r < 0.°75$	428	1:1.07:20.01	0.°5	48.°84
$r < 1.°00$	671	1:1.03:14.01	0.°4	64.°88
$r < 1.°25$	927	1:1.03:11.19	0.°4	67.°84
$r < 1.°50$	1177	1:1.13:9.59	0.°2	59.°54
$r < 1.°75$	1399	1:1.23:8.70	0.°2	60.°10
$r < 2.°00$	1568	1:1.30:8.00	0.°1	64.°87
$r < 2.°25$	1755	1:1.34:7.22	0.°3	68.°78
$r < 2.°50$	1845	1:1.36:6.89	0.°4	70.°80
$r < 2.°75$	1892	1:1.34:6.57	0.°4	73.°70
$r < 3.°00$	1904	1:1.33:6.47	0.°3	74.°40

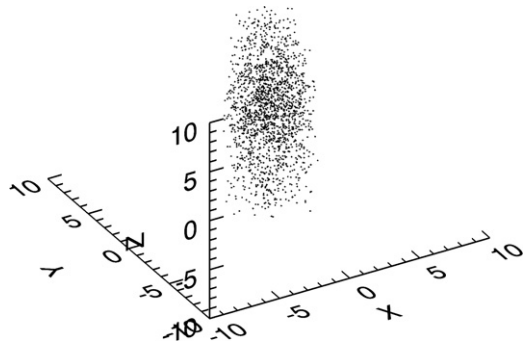

Figure 14. x, y, and z values of the whole sample of RRLS are plotted.

6.2. Red Clump Stars

From the previous sections, we found that the RC stars and RRLS occupy a similar volume of the SMC. Hence we can apply the method of inertia tensor to the RC stars for the estimation of the parameters of the ellipsoidal component of the SMC. First, we apply this method to the (x, y) coordinates of the 553 sub-regions of the SMC. Here each (x, y) pair represents the coordinates of a sub-region. We weighted it using the number of RC stars identified in that region to obtain the axes ratio. We find that the RC distribution in the SMC is elongated with an axes ratio of 1:1.48 and the position angle of the major axis is 55.°3. Now we applied the same procedure to the (x, y, z) system of the RC stars. In the case of RRLS, we took the distance of the individual RRLS with respect to the mean distance as the z coordinate, but in the case of RC stars we only have the mean magnitudes corresponding to the mean distances to the sub-regions. The mean magnitude of a region in the ellipsoidal or nearly spheroidal system is the average of the magnitude of symmetrically distributed RC stars. In order to obtain the real RC distribution we did the following. After subtracting the average extinction, we obtained the magnitude distribution of the RC stars for each sub-region. Using the method explained earlier in Section 3.1, we estimated the peak and the width of the magnitude distribution for each sub-region and eventually the width corresponding to depth. The depth (front to back distance) of the RC stars in a region is the measure of the extent to which the RC stars in that region are distributed. Most of the RC stars in a sub-region are at the mean distance obtained for that sub-region and the remaining are distributed within the depth of the region. We assume the distribution to be symmetric with respect to the mean distance to that sub-region. Initially, we took the I_0 values of the bins within 1σ width and converted them into z-distances. As we have the number of stars in each bin we weighted and applied the inertia tensor analysis to the x, y, and z coordinates.

Earlier we found that the RC and RR Lyrae depth distributions are similar. Also, from Figures 10 and 11 we can see that the RR Lyrae distribution extends up to 3σ–4σ depth. Hence we can take the z component to extend up to higher sigma levels (2σ, 3σ, 3.5σ, 4σ) to understand the real RC distribution in the SMC. We applied the inertia tensor analysis using z components which extend up to 2σ, 3σ, 3.5σ, and 4σ. The parameters obtained are given in Table 3. From the table we can see that the orientation measurements of the ellipsoidal component of the SMC using RC stars, where the z component extends up to 3.5σ, are similar to the values obtained for the RR Lyrae distribution excluding the northwestern fields. As we removed the regions with RC stars less than 400, the northwestern fields are not included in the analysis. The axes ratio and the angle i match well with the ellipsoidal parameters of the SMC estimated using the distribution of the RRLS. The position angle, ϕ, estimated using the RC stars and RRLS is slightly different.

Table 3
Orientation Measurements of the Ellipsoidal Component of the SMC Using the RC Stars

Data	Axes Ratio	i	ϕ
RC stars within 1σ depth	1:1.49:3.08	4.°22	55.°7
RC stars within 2σ depth	1:1.48:5.26	1.°23	55.°4
RC stars within 3σ depth	1:1.48:7.10	0.°68	55.°6
RC stars within 3.5σ depth	1:1.48:7.88	0.°58	55.°5
RC stars within 4σ depth	1:1.48:8.58	0.°49	55.°4

Table 4
Orientation Measurements of the Ellipsoidal Component of the SMC Using the RC Stars and the RRLS in the Same Region

Data	Axes Ratio	i	ϕ
1654 RRLS	1:1.46:8.04	0.°50	58.°3
RC stars within 3.5σ depth	1:1.48:7.88	0.°58	55.°5

Note. Excluding the northwestern fields and the edges of the data.

Based on the analysis described above, we can say that the RC stars in the SMC are distributed in an ellipsoidal system with an axes ratio of 1:1.48:7.88. The position angle, ϕ,is 55.°5. The longest axis Z' which is perpendicular to the $X'Y'$ plane (obtained by the counterclockwise rotation of the XY plane with an angle 55.°5 with respect to the Z-axis) is inclined with the Z-axis with an angle of 0.°58. The inclination of the Z'-axis with the line of sight is very small and we can assume the longest axis to be almost along the line of sight.

6.3. Comparison of the Structural Parameters Obtained from Both Populations

The quantities estimated in this analysis strongly depend on the data coverage. In order to compare the axes ratio and the orientation measurements obtained from both populations, it is important to take the sample of both population of stars from the same region. In the case of the RC stars, regions that include the northwestern fields and also regions in the edges of the data set are omitted based on the selection criteria. Such a truncation of the data is not done in the case of the RRLS. Only the RRLS which are possible Galactic objects are removed from the analysis. These stars are not concentrated on a particular region but are scattered. If we remove the RRLS in the northwestern fields and the edges of the data, then the sample of RRLS covers nearly the same region as the RC stars' sample. We used the RRLS within the box of size -1.8 to 1.8 in both the X- and Y-axes. Thus the RRLS in the edges of the data set and in the northwestern fields are nearly removed. Then we estimated the parameters using this sample of the RRLS and the values are given in Table 4. From the table we can see that when the sample of both populations is taken from similar regions of the SMC the estimated parameters match well.

6.4. The Actual Structure of the SMC

We find that the $Z' \sim Z$ axis is the longest axis in the analysis of both the RRLS and the RC stars. The reason for such a result is mainly the coverage of the SMC. The studied data cover only the central regions thus restricting the coverage in the XY plane. On

Table 5
Estimated Structural Parameters with Equal Extent in All Three Axes

Data	Number of RRLS	Axes Ratio	ϕ (deg)	i (deg)
$\rho < 2.0$	344	1:1.17:1.28	67.5	4.2
$\rho < 2.5$	540	1:1.24:1.39	69.5	3.3
$\rho < 3.0$	730	1:1.33:1.61	70.2	2.6

the other hand, the full Z-direction is sampled. Hence the present view of the SMC based on our axes ratio is like viewing only the central part of a sphere along the Z-axis. Such a perspective will give an elongated Z-axis. This is clear from Figure 14. In order to test whether the $z' \sim z$ axis is due to the viewing perspective, we have sampled the data similarly along the three axes. The extent of the sample along all three axes can be made equal by taking the data only within spherical radii (ρ) of 2°, $2.^\circ5$, and 3° from the center. We took the RRLS stars within these different radii and estimated the structural parameters. The estimated parameters are given in Table 5. An elongation in the NE–SW axis is seen as suggesting that the elongation of the RRLS in the NE–SW is a real feature. The decrease in the relative length of the z'-axis is expected as the selection mentioned above removes relatively more stars along the z'-direction than in the x' and y' directions. From Table 5 we can see that the inclination of the longest axis with the line-of-sight axis decreases from inner to outer radii. The finite XY coverage further restricts analysis of this trend. The very small value of i (given in Tables 2 and 4) estimated from the analysis of all the RRLS, including those at larger z-distances from the center, indicates that the decreasing trend of i is also continued to outer radii. In Table 5, we can also see an increase in ϕ and the relative length of the y'-axis from inner to outer regions. From Section 6.1 and Table 2, we can understand that these two quantities are dependent on the choice of the centroid of the system. So we cannot definitely say anything more about this trend. Another important result to be noted from Table 5 is that even though the z'-axis is the longest of the three, the values of the longest and the second longest (y') axes are comparable. This suggests that when the coverage along all three axes becomes comparable, the structure of the SMC is spheroidal or slightly ellipsoidal.

The above analysis indicates that the XY extent of the SMC up to which stellar populations are studied/detected plays an important role in understanding the actual structure of the SMC and hence the estimation of the structural parameters. The tidal radius estimates give the radial extent to which the stellar populations are bound to the SMC or to which they are expected to be found. Gardiner & Noguchi (1996) estimated the tidal radius of the SMC to be ∼5 kpc. Later, Stanimirović et al. (2004) suggested the tidal radius of the SMC to be 4–9 kpc. The estimations obtained in our study from the radial density and surface density profiles of the RC stars, given in Table 1, suggest the tidal radius to be 7–12 kpc. There are many recent studies which found old and intermediate stellar populations in the outer regions. Noël et al. (2007) found that up to 6.5 kpc from the SMC center, the galaxy is composed of both intermediate-age and old populations without an extended halo. De Propris et al. (2010) estimated the SMC edge in the eastern direction to be around 6 kpc from the survey of red giant stars in 10 fields in the SMC. A very recent photometric survey of the stellar periphery of the SMC by Nidever et al. (2011) found the presence of old and intermediate-age populations up to at least 9 kpc. The above-mentioned observational studies and tidal radius estimates suggest that the full extent of the SMC in the XY plane ($2\times9 = 18$ kpc) is of the order of the front to back distance estimated (14 kpc) along the Z-axis. We found in earlier sections that the inner SMC is slightly elongated in the NE–SW direction. Thus we suggest that the actual structure of the SMC is spheroidal or slightly ellipsoidal. Better estimates of the structural parameters can be obtained with a data set of larger sky coverage. In the following section, we combine previous studies and suggest an evolutionary model for the SMC.

7. DISCUSSION

Bekki & Chiba (2008) suggested that the SMC may be formed due to a dwarf–dwarf merger, resulting in a stellar spheroidal component and a gaseous disk component, happened before the formation of the Milky-Way–LMC–SMC system. They also suggest that since stellar populations formed before the merger event should have dynamically hot kinematics, the youngest age of stellar populations that show both spheroidal distributions and no or little rotation can correspond to the epoch when the merger occurred. As the merger event should evoke a large-scale star formation event in the galaxy, the epoch of the merger can also be traced from the enhancements seen in the star formation history of the SMC.

The most comprehensive study of the star formation history of the SMC is presented by Harris & Zaritsky (2004). They derived the global star formation history of the SMC. They found that there was a significant epoch of star formation up to 8.4 Gyr ago when 50% of the stars were formed, followed by a long quiescent period in the range 3 Gyr < age < 8.4 Gyr, and a more or less continuous period of star formation starting 3 Gyr ago and extending to the present. They also found three peaks in the star formation rate, at 2–3 Gyr, 400 Myr, and 60 Myr ago. Their CMDs do not go deep enough to derive the full star formation history from the information on the main sequence. Obtaining CMDs reaching the oldest main-sequence turnoff is essential in order to properly constrain the intermediate-age and old populations (Gallart et al. 2005). As we study the intermediate-age and old stellar populations in the SMC, here we compare the star formation studies performed based on the CMDs that reach the oldest main-sequence turnoffs. These studies go deeper and hence have smaller fields of view. Dolphin et al. (2001), Chiosi & Vallenari (2007), and Noël et al. (2009) have conducted such studies and obtained the star formation history of the SMC.

Dolphin et al. (2001) found a broad peak of star formation between 5 and 8 Gyr ago. Chiosi & Vallenari (2007) found two main episodes of star formation, at 300–400 Myr and between 3–6 Gyr. They also found that the star formation rate was low until ≈ 6 Gyr ago, when only a few stars were formed. Noël et al. (2009) found star formation enhancements at two intermediate ages, a conspicuous one peaked at 4–5 Gyr old in all fields and a less significant one peaked at 1.5–2.5 Gyr old in all fields. The enhancement at old ages with the peak at 10 Gyr old is seen in all fields, but in the western fields, this old enhancement is split into two at 8 Gyr old and at 12 Gyr old. Their farthest field is at 4.5 kpc. All these studies show an enhancement in the star formation in the SMC around 4–5 Gyr ago.

If the 4–5 Gyr global star formation in the SMC is assumed to be due to a dwarf–dwarf merger, then according to the merger model, the merged galaxy will settle down within 1–3 Gyr (Lotz et al. 2008). This scenario will then demand a spheroidal component well mixed with stars older than 2 Gyr. Our results find that the old population (RRLS, age >9 Gyr) and the intermediate-age component (RC stars, age = 2–9 Gyr) seem to

occupy a similar volume, suggesting that stars older than 2 Gyr are in a well-mixed ellipsoid.

Tsujimoto & Bekki (2009) proposed that the evidence of a major merger event in the SMC is imprinted in the age–metallicity relation as a dip in [Fe/H]. They predicted that the major merger with a mass ratio of 1:1 to 1:4 occurred at ∼7.5 Gyr ago in the SMC. Based on this model they could reproduce the abundance distribution function of the field stars in the SMC. As they could not correlate a peak in the star formation history of the SMC at the epoch of the merger they suggested that the major merger which occurred in the SMC at 7.5 Gyr ago did not trigger a major starburst due to some physical reasons but proceeded with a moderate star formation. Noël et al. (2009) did not find a dip in the age–metallicity relation of the SMC, which Tsujimoto & Bekki (2009) claimed to detect and suggested as the imprint of a major merger at 7.5 Gyr ago. Again if this merger event in the SMC at 7.5 Gyr old is the reason for the kinematical and morphological differences between the young and old stars then we cannot expect to find stars younger than 4–5 Gyr in the spheroidal/ellipsoidal distribution. As we find RC stars with an age range of 2–9 Gyr in the spheroidal/ellipsoidal distribution, we propose a merger event which started around 4–5 Gyr ago as the reason for the observed distribution of stars in the SMC.

A wider and larger future photometric (OGLE IV) and spectroscopic surveys which will cover both the inner and outer regions of the SMC will help to understand the complete structure and kinematics of the SMC.

8. CONCLUSIONS

1. The dereddened I_0 magnitudes of the RC stars and RRLS are used to determine the relative positions of the regions in the SMC with respect to the mean distance and these suggest that either the population of the RC stars and RRLS in the northeastern regions are different and/or the northeastern part of the SMC is closer to us.
2. The line-of-sight depth of the SMC estimated using the RC stars and the RRLS is found to be ∼14 kpc. The depth profiles of both populations look similar, indicating that these two populations are located in a similar volume of the SMC.
3. The surface density distribution and the radial density profile of the RC stars suggest that they are distributed in a nearly spheroidal system. The tidal radius estimated for the SMC system is ∼7–12 kpc. An elongation from NE–SW is also seen in the surface density map of the RC stars in the SMC.
4. The observed SMC is approximated as a triaxial ellipsoid and the structural parameters, like the axes ratio, inclination, i, of the longest axis with the line of sight, and the position angle, ϕ, of the projection of the ellipsoid on the plane of the sky, are estimated using the inertia tensor analysis. From the analysis of the RC stars and RRLS in the same region of the SMC the parameters estimated turned out to be very similar. The estimated parameters are very much dependent on the data coverage.
5. The study of data only within concentric spheres of radii of 2°, 2.°5, and 3° from the center, where the extent in all three axes becomes equal, shows that the relative lengths of the z'- and y'-axes are comparable. We estimated an axes ratio of 1:1.33:1.61 with a 2.°6 inclination of the longest axis with the line of sight from the analysis of RRLS within 3°in the X-, Y-, and Z-axes. The position angle of the projection of the ellipsoid on the sky obtained is 70.°2. Our tidal radius estimates and various observational studies of the outer regions suggest that the full extent of the SMC in the XY plane is similar to the front to back distance estimated along the line of sight. These results suggest that the actual structure of the SMC is spheroidal or slightly ellipsoidal.
6. We propose that the SMC experienced a merger with another dwarf galaxy about 4–5 Gyr ago, and the merger process was completed in another 2–3 Gyr. This resulted in a spheroidal distribution comprising stars older than 2 Gyr.

Smitha Subramanian acknowledges the financial support provided by the Council of Scientific and Industrial Research (CSIR), India through SRF grant 09/890(0002)/2007-EMR-I. The authors thank the OGLE team for making the data available in public. Thanks to Indu.G for her help in plotting figures. The authors thank the anonymous referee for the constructive suggestions which improved the manuscript.

APPENDIX

INERTIA TENSOR ANALYSIS

The moment of inertia of a body characterizes the mass distribution within the body. For any rotating three-dimensional system, we can compute the moment of inertia about the axis of rotation, which passes through the origin of a local reference (XYZ) frame, using the inertia tensor. The origin of the system is the center of mass of the body. Consider a system made up of i number of particles, each particle with a mass m. For each particle the (x, y, and z) coordinates with respect to the center of mass are known. Then, the moment of inertia tensor, I, of the system is given by

$$I = \begin{pmatrix} I_{xx} & I_{xy} & I_{xz} \\ I_{yx} & I_{yy} & I_{yz} \\ I_{zx} & I_{zy} & I_{zz} \end{pmatrix},$$

where

$$\begin{aligned} I_{xx} &= \Sigma_i m_i (y_i^2 + z_i^2) \\ I_{yy} &= \Sigma_i m_i (x_i^2 + z_i^2) \\ I_{zz} &= \Sigma_i m_i (x_i^2 + y_i^2) \\ I_{xy} = I_{yx} &= \Sigma_i m_i (x_i + y_i) \\ I_{yz} = I_{zy} &= \Sigma_i m_i (y_i + z_i) \\ I_{xz} = I_{zx} &= \Sigma_i m_i (x_i + z_i). \end{aligned}$$

The components, I_{xx}, I_{yy}, and I_{zz} are called the moments of inertia while I_{xy}, I_{yx}, I_{xz}, I_{zx}, I_{yz}, and I_{zy} are the products of inertia. These components given above are basically specific to the local reference frame and reflect the mass distribution within the system in relation to the local reference frame. If we align the axes of the local reference frame in such a way that the mass of the system is evenly distributed around the axes then the product of inertia terms vanish. This would mean the transformation of the local reference frame (XYZ) to a system ($X'Y'Z'$). In the new frame of reference, inertia tensor I' is given by

$$I' = \begin{pmatrix} I_{x'x'} & 0 & 0 \\ 0 & I_{y'y'} & 0 \\ 0 & 0 & I_{z'z'} \end{pmatrix}.$$

The terms $I_{x'x'}$, $I_{y'y'}$, and $I_{z'z'}$ are the nonzero diagonal terms of the inertia tensor in the new reference frame ($X'Y'Z'$) and are called the principal moments of inertia of the body. The three axes in the new reference frame are called the principal axes of the body.

To determine the principal axes of the system, we have to diagonalize the inertia tensor I, which is obtained with respect to the local reference frame. The diagonalization of the inertia tensor provides three eigenvalues (λ_1, λ_2, and λ_3) which correspond to the moments of inertia ($I_{x'x'}$, $I_{y'y'}$, and $I_{z'z'}$) about the principal axes. For each eigenvalue we can compute the corresponding eigenvector. The eigenvectors corresponding to each eigenvalue are given as $e_{\lambda_1} = e_{11}\,i' + e_{12}\,j' + e_{13}\,k'$, $e_{\lambda_2} = e_{21}\,i' + e_{22}\,j' + e_{23}\,k'$, and $e_{\lambda_3} = e_{31}\,i' + e_{32}\,j' + e_{33}\,k'$, where i', j', and k' are unit vectors along the X'-, Y'-, and Z'-axes, respectively. The transformation of the XYZ system to $X'Y'Z'$ can be obtained using the transformation matrix, T, which is made up of the nine components of the three eigenvectors. The transformation matrix, T, is given by

$$T = \begin{pmatrix} e_{11} & e_{21} & e_{31} \\ e_{12} & e_{22} & e_{32} \\ e_{13} & e_{23} & e_{33} \end{pmatrix}.$$

From the eigenvalues and the transformation matrix, the axes ratio and the orientation of the characteristic ellipsoid that best describes the spatial distribution of the particles in the system can be obtained. As the moment of inertia of a system characterizes the resistance of the system to rotation, the component of the moment of inertia along the major axis of the system will be least and it will be the maximum along the minor axis. Thus the three eigenvalues which represent the moments of inertia of the three axes (such that $I_{x'x'} > I_{y'y'} > I_{z'z'}$) of the ellipsoid can be written as

$$I_{x'x'} = M(a^2 + b^2)$$
$$I_{y'y'} = M(a^2 + c^2)$$
$$I_{z'z'} = M(b^2 + c^2),$$

where a, b, and c are the semi-axes of the ellipsoid such that $a > b > c$ and M is the total mass of the system. Using the above relations we can estimate the axes ratio of the ellipsoid which best describes the spatial distribution of the particles in the system. The transformation matrix, T, describes the spatial directions or the orientation of the ellipsoid with respect to the local reference frame.

REFERENCES

Bekki, K., & Chiba, M. 2008, ApJ, 679, L89
Borissova, J., Rejkuba, M., Minniti, D., Catelan, M., & Ivanov, V. D. 2009, A&A, 502, 505
Caldwell, J. A. R., & Coulson, I. M. 1985, MNRAS, 212, 879
Caldwell, J. A. R., & Coulson, I. M. 1986, MNRAS, 218, 223
Chiosi, E., & Vallenari, A. 2007, A&A, 466, 165
Cioni, M., Habing, H. J., & Israel, F. P. 2000, A&A, 358, L9
Cioni, M.-R. L., Girardi, L., Marigo, P., & Habing, H. J. 2006, A&A, 452, 195
Clementini, G., Gratton, R., Bragaglia, A., et al. 2003, AJ, 125, 1309
Cole, A. A. 1998, ApJ, 500, L137
Crowl, H. H., Sarajedini, A., Piatti, A. E., et al. 2001, AJ, 122, 220
De Propris, R., Rich, R. M., Mallery, R. C., & Howard, C. D. 2010, ApJ, 714, L249
Dolphin, A. E., Walker, A. R., Hodge, P. W., et al. 2001, ApJ, 562, 303
Dopita, M. A., Lawrence, C. J., Ford, H. C., & Webster, B. L. 1985, ApJ, 296, 390
Evans, C. J., & Howarth, I. D. 2008, MNRAS, 386, 826
Gallart, C., Zoccali, M., & Aparicio, A. 2005, ARA&A, 43, 387
Gardiner, L. T., & Hawkins, M. R. S. 1991, MNRAS, 251, 174
Gardiner, L. T., & Noguchi, M. 1996, MNRAS, 278, 191
Girardi, L., & Salaris, M. 2001, MNRAS, 323, 109
Glatt, K., Grebel, E. K., Sabbi, E., et al. 2008, AJ, 136, 1703
Graham, J. A. 1975, PASP, 87, 641
Grieve, G. R., & Madore, B. F. 1986, ApJS, 62, 427
Groenewegen, M. A. T. 2000, A&A, 363, 901
Harris, J., & Zaritsky, D. 2004, AJ, 127, 1531
Harris, J., & Zaritsky, D. 2006, AJ, 131, 2514
Haschke, R., Grebel, E. K., & Duffau, S. 2011, AJ, 141, 158
Hatzidimitriou, D., Cannon, R. D., & Hawkins, M. R. S. 1993, MNRAS, 261, 873
Hatzidimitriou, D., Croke, B. F., Morgan, D. H., & Cannon, R. D. 1997, A&AS, 122, 507
King, I. 1962, AJ, 67, 471
Lotz, J. M., Jonsson, P., Cox, T. J., & Primack, J. R. 2008, MNRAS, 391, 1137
Maragoudaki, F., Kontizas, M., Morgan, D. H., et al. 2001, A&A, 379, 864
Massey, P., Lang, C. C., Degioia-Eastwood, K., & Garmany, C. D. 1995, ApJ, 438, 188
Nidever, D. L., Majewski, S. R., Munoz, R. R., et al. 2011, ApJ, 733, L10
Noël, N. E. D., Aparicio, A., Gallart, C., et al. 2009, ApJ, 705, 1260
Noël, N. E. D., Gallart, C., Costa, E., & Méndez, R. A. 2007, AJ, 133, 2037
Olsen, K. A. G., & Salyk, C. 2002, AJ, 124, 2045
Pagel, B. E. J., & Tautvaisiene, G. 1998, MNRAS, 299, 535
Paz, D. J., Lambas, D. G., Padilla, N., & Merchán, M. 2006, MNRAS, 366, 1503
Pejcha, O., & Stanek, K. Z. 2009, ApJ, 704, 1730
Sarajedini, A. 1999, AJ, 118, 2321
Schlegel, D. J., Finkbeiner, D. P., & Davis, M. 1998, ApJ, 500, 525
Smith, H. A., Silbermann, N. A., Baird, S. R., & Graham, J. A. 1992, AJ, 104, 1430
Soszyński, I., Udalski, A., Szymanski, M., et al. 2002, Acta Astron., 52, 369
Soszyński, I., Udalski, A., Szymański, M. K., et al. 2010, Acta Astron., 60, 165
Stanek, K. Z., Zaritsky, D., & Harris, J. 1998, ApJ, 500, L141
Stanimirović, S., Staveley-Smith, L., & Jones, P. A. 2004, ApJ, 604, 176
Subramaniam, A. 2003, ApJ, 598, L19
Subramaniam, A. 2005, A&A, 430, 421
Subramaniam, A. 2006, A&A, 449, 101
Subramanian, S., & Subramaniam, A. 2009, A&A, 496, 399
Subramanian, S., & Subramaniam, A. 2010, A&A, 520, A24
Suntzeff, N. B., Friel, E., Klemola, A., Kraft, R. P., & Graham, J. A. 1986, AJ, 91, 275
Tosi, M., Gallagher, J., Sabbi, E., et al. 2008, in IAU Symp. 255, Low-Metallicity Star Formation: From the First Stars to Dwarf Galaxies, ed. L. K. Hunt, S. Madden, & R. Schneider (Cambridge: Cambridge Univ. Press), 381
Tsujimoto, T., & Bekki, K. 2009, ApJ, 700, L69
Udalski, A. 1998, Acta Astron., 48, 383
Udalski, A., Soszyński, I., Szymański, M. K., et al. 2008, Acta Astron., 58, 329
van der Marel, R. P., & Cioni, M. 2001, AJ, 122, 1807
van der Marel, R. P., Kallivayalil, N., & Besla, G. 2009, in IAU Symp. 256, The Magellanic System: Stars, Gas and Galaxies, ed. J. T. van Loon & J. M. Oliveira (Cambridge: Cambridge Univ. Press), 81
Weinberg, M. D., & Nikolaev, S. 2001, ApJ, 548, 712
Zaritsky, D., Harris, J., Grebel, E. K., & Thompson, I. B. 2000, ApJ, 534, L53